Supporting Information for Prediction of Novel Gallium-Sulfur Compositions Under Pressure

Reza Shahsavari,[†,‡] Sylvain Pitié,[†] Somayeh Faraji,[†] Lewis J. Conway,[¶] Chris J. Pickard,[¶] Seyed J. Hashemifar,[§] Alireza Shahidi,[‡] and Gilles Frapper[*,†]

†*Applied Quantum Chemistry Group, E4 team, IC2MP UMR 7285, Université de Poitiers – CNRS, 4, rue Michel Brunet TSA 51106 – 86073, Poitiers, France*

‡*Department of Mechanical Engineering, Isfahan University of Technology, Isfahan 84156-83111, Iran*

¶*Department of Materials Science & Metallurgy, University of Cambridge, 27 Charles Babbage Road, Cambridge, CB3 0FS, UK*

§*Department of Physics, Isfahan University of Technology, Isfahan 84156-83111, Iran*

E-mail: gilles.frapper@univ-poitiers.fr

Contents

S1 Methodology Details

S1.1 Evolutionary Algorithm (USPEX).

We provide here the technical details of the USPEX evolutionary structural searches with a brief description of the fixed-composition evolutionary algorithm (EA). USPEX[1–4] (Universal Structure Predictor: Evolutionary Xtallography) is a structure prediction algorithm developed by the A.R. Oganov laboratory in 2004 that employs a global evolutionary search approach. (For more information on USPEX, visit `http://uspex-team.org/en/uspex/overview`). In this project, the evolutionary algorithm (EA) code has been integrated with VASP[5,6] (Vienna *Ab initio* Simulation Package) to perform DFT (density functional theory) structure relaxation. This involves optimizing the shape, volume, and atomic positions of the system using VASP. To discover stable ground-state structures and compositions in the binary Ga-S system, a variable-composition EA implemented in the USPEX code is utilized. By using this approach, we are able to explore the configurational, structural, and compositional spaces of Ga_xS_y (where x and y are positive integers) and identify the local minima on the potential energy surface (PES). The variable composition EA is carried out at specified pressures of 0, 10, 20, 40, 60, 80, 100 GPa. Finally, fixed composition EA structural searches are conducted for the designated (x, y) compositions and pressures with four different unit formulas (Z = 1-4) to verify that the proposed structures are, in fact, the most energetically favorable on the PES. In the evolutionary algorithm implemented in USPEX, five operators are utilized to produce new candidate structures. These operators include heredity, softmodemutation, transmutation, randSym, and randTop. In our work, heredity is the most heavily-weighted operator, with a weight of 0.5 in the first generation. The minimum and maximum percentages of structures generated per generation for each operator are predetermined, with heredity having a minimum of 0.1 and a maximum of 1.0. Similarly, softmodemutation, randSym, and randTop have minimums and maximums of 0.1 and 0.05, respectively, while transmutation has a minimum of 0.05 and a maximum of 1.0. The weight

of transmutation in the first generation is 0.2. In the first generation, 60 candidate structures were generated, and all subsequent generations consisted of 40 structures. Structures are removed from the pool based on their fitness, which is determined by the computed free enthalpy obtained from *ab initio* total energy calculations using VASP. The remaining structures are used as parent structures to generate the next generation. The simulation allows a maximum of 60 generations, but it may terminate earlier if the best structure remains unchanged for 10 consecutive generations. Typically, the EA search converges within 13 generations, meaning approximately 540 structures are optimized in total. As previously stated, VASP is utilized as an external code for structure relaxations and energy calculations in the USPEX search. This involves the use of 5 INCAR files (5 steps per phase). To ensure that a global minimum is reached, each fixed-composition USPEX job is run at least twice.

S1.2 Density Functional Theory (DFT) Computational Details

S1.2.1 DFT Framework of USPEX Calculations.

The calculations in this study were carried out using the first-principles approach, with the projected-augmented-wave (PAW) method[7,8] implemented in VASP (version 5.4.4). In USPEX simulations, the Perdew-Burke-b Ernzerhof (PBE) approach[9] is utilized to account for the exchange-correlation energy. The PAW potentials for Gallium and Sulfur atoms with a radius of 2.3 au and 1.9 au, respectively, are utilized within the generalized gradient approximation (GGA). Additionally, pseudopotentials employing the $3d^{10}4s^24p^1$ and $3s^23p^4$ valence configurations are employed for Ga and S, respectively. Typically, optimizing each crystalline structure necessitates a sequence of 5 steps, each with progressively greater convergence accuracy, which entails using 5 separate INCAR files. The parameters and criteria linked with VASP calculations are related to the final (5th) step, which offers the highest level of accuracy. For wavefunction expansion, a kinetic cutoff energy of 520 eV is employed, along with a Monkhorst-Pack k mesh grid featuring a spacing of $2\pi \times 0.02$ Å^{-1}.

S1.3 *Ab Initio* Random Structure Search (AIRSS)

The method of *Ab Initio* Random Structure Searching (AIRSS)[10,11] is an uncomplicated and greatly parallel technique for predicting structures was introduced in 2006 by C.J. Pickard laboratory and its philosophy more extensively discussed in 2011. (For more information on AIRSS, visit `https://www.mtg.msm.cam.ac.uk/Codes/AIRSS`). Random structures, are initially created and subsequently relaxed to nearby local energy minima. In this project, the random search code has been integrated with repose code, which performs local structural optimisation of atomic configurations through the utilization of Ephemeral Data Derived Potentials (EDDPs).[12] Fixed composition random structural searches are conducted for the designated (x, y) compositions and pressures with Number of formula units (Z = 1-8) to verify that the proposed structures are, in fact, the most energetically favorable on the PES. A substantial number of structures were generated and optimized to investigate the Ga–S binary system. The convex hull at each pressure was explored using AIRSS-based EDDP methods. Refer to Figures S1(a), S2(a), S3(a), and S4(a) for the corresponding hulls. The distance from the hull, expressed in meV/atom, is shown in Figures S1(b), S2(b), S3(b), and S4(b).

S1.3.1 Input Parametres Chosen for the EDDP Training

Table S1: The Input Parameters Chosen for the EDDP Training as well as the Underlying DFT Calculations in Ga-S System.

Parameter	Ga-S system
DFT Parameters	
Energy cutoff [eV]	520.0
XC functional	PBE
Structure Building Parameters	
Minimum interatomic distance [Å]	0.5-2
Volume per atom [Å^3]	Ga: 10-18
	S: 9-26
EDDP Training Parameters	
r_c [Å]	6
Number of exponents	6
Highest body order	3
Number of nodes in hidden layer	5
Number of random structures	8000
Number of cycles	8
Number of local minima per cycle	110
Number of shakes per local minimum	10
Total number of structures	17680
Pressure range [GPa]	0-100
Number of EDDPs generated	256
Number of EDDPs selected by NNLS	15
MAE [meV/atom]	46.78

S1.3.2 Crystal Structure Prediction Exploration

A large number of structures were generated and optimized to investigate the Ga-S binary. The hull from each pressure was explored using AIRSS-based EDDPs. Refer to Figures S1.(a), S2.(a), S3.(a), and S4.(a). The distance from the hull in meV/atom is provided in Figures S1.(b), S2.(b), S3.(b), and S4.(b).

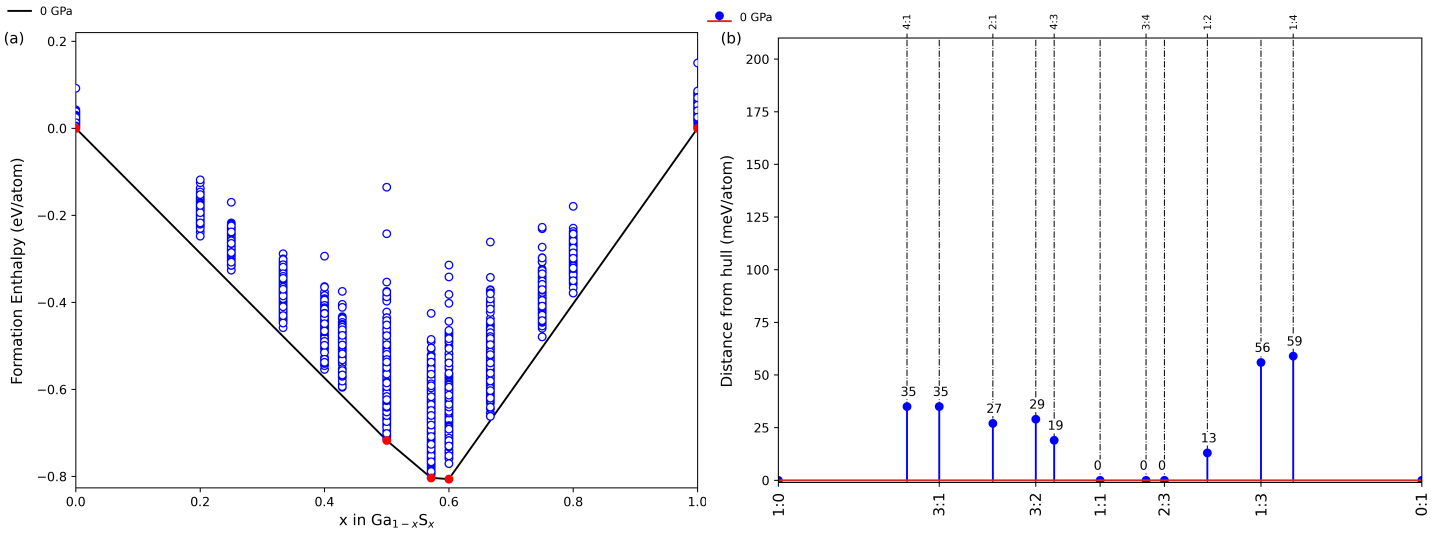

Figure S1: (a) Convex hull diagram for the Ga-S system and (b) distance from hull at 0 GPa (EDDP search).

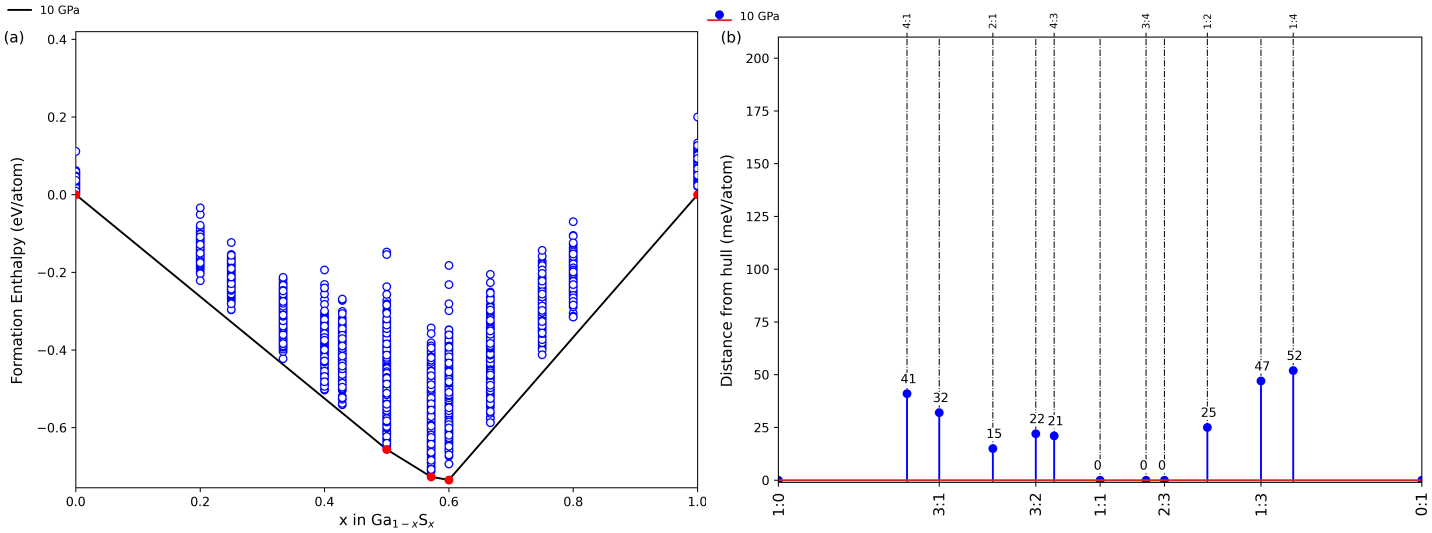

Figure S2: (a) Convex hull diagram for the Ga-S system and (b) distance from hull at 10 GPa (EDDP search).

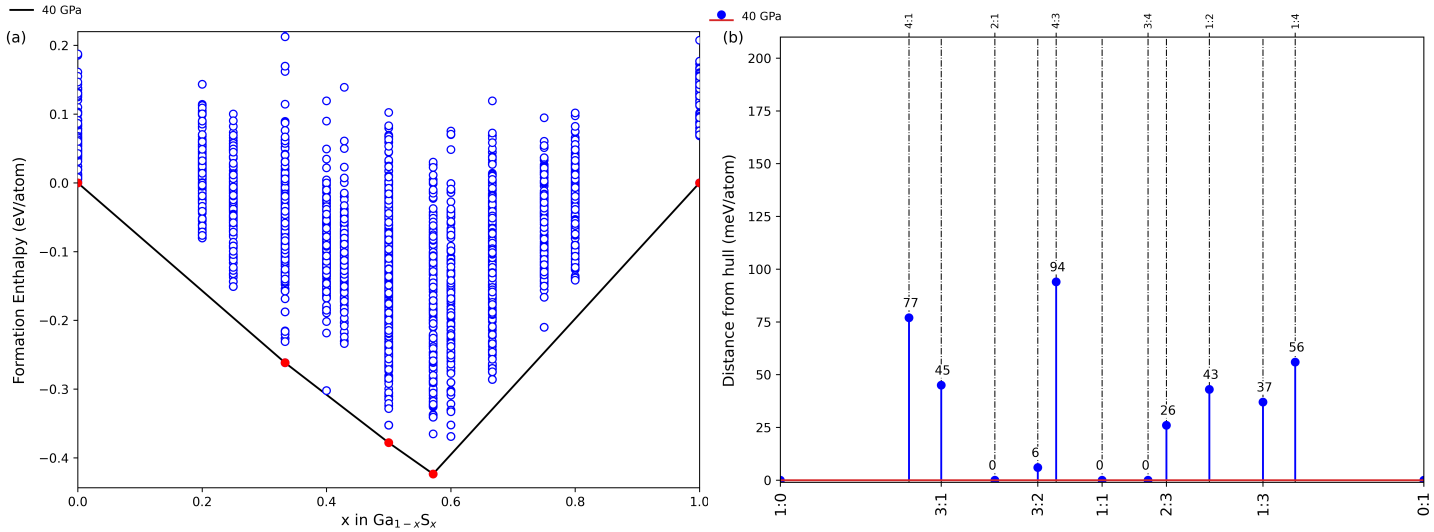

Figure S3: (a) Convex hull diagram for the Ga-S system and (b) distance from hull at 40 GPa (EDDP search).

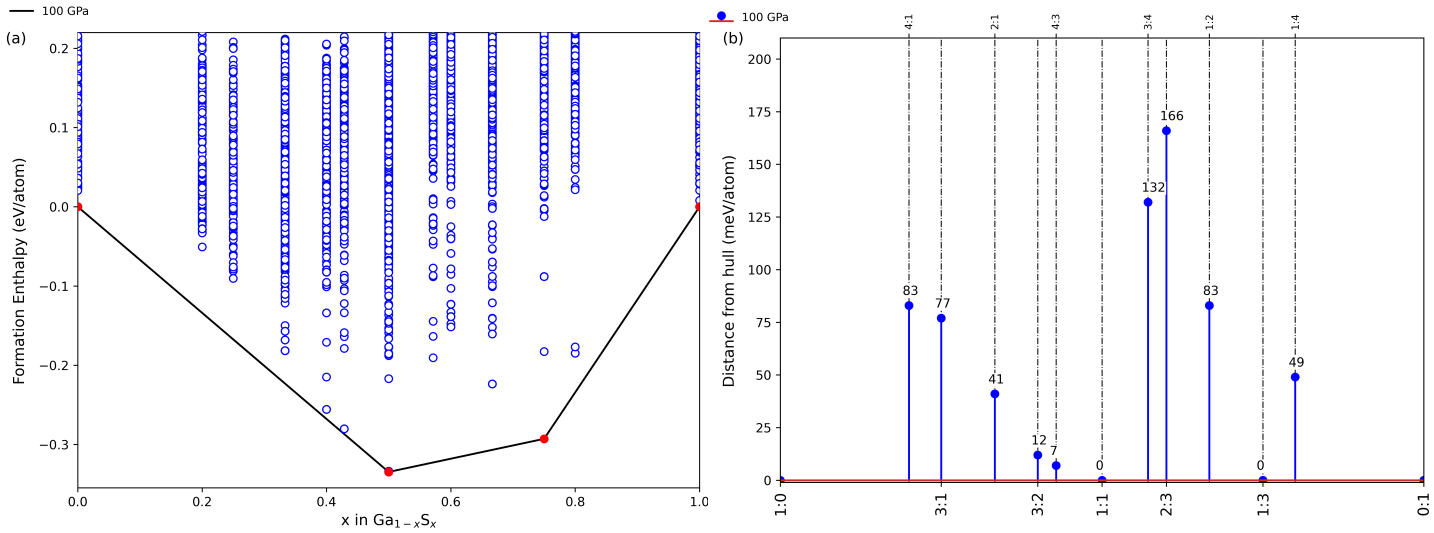

Figure S4: (a) Convex hull diagram for the Ga-S system and (b) distance from hull at 100 GPa (EDDP search).

S1.3.3 Comparative Analysis of USPEX-Based DFT and AIRSS-Based EDDP Results

Crystal structure searches were systematically carried out using USPEX (DFT-based) and AIRSS (EDDP-based) methods. The ground state structures obtained were fully optimized at the DFT GGA PBE level of theory, and the results are presented and compared in tabular form.

Table S2: USPEX-Based DFT and AIRSS-Based EDDP Results.

Structure	**Pressure (GPa)**	**Method**	**Space group**	**Z**	**Enthalpy (eV/atom)**
		USPEX	$I4_1/amd$	4	-1.499
Ga_2S	20	AIRSS	$C2/m$	4	-1.490
		USPEX	$P6_3/mmc$	8	-4.165
GaS	0	AIRSS	$P6_3/mmc$	4	-4.165
		USPEX	$C2/m$	4	-2.888
GaS	10	AIRSS	$I4/mmm$	4	-2.840
		USPEX	R-$3/m$	3	1.554
GaS	60	AIRSS	R-$3/m$	3	1.555
		USPEX	$C2/m$	2	-2.987
Ga_3S_4	10	AIRSS	$P2/m$	3	-2.987
		USPEX	$Imm2$	2	-4.296
Ga_2S_3	0	AIRSS	Cc	2	-4.296
		USPEX	$R3/m$	3	-3.036
Ga_2S_3	10	AIRSS	$R3/m$	1	-3.022
		USPEX	R-$3/m$	2	1.410
Ga_2S_3	60	AIRSS	$C2/m$	3	1.412
		USPEX	$C2/m$	4	-2.989
GaS_2	10	AIRSS	$C2/m$	2	-2.989

S1.4 Post Crystal Structure Prediction Treatment

To optimize the selected phases, we tested other functionals. We finally chose to treat the weak dispersion forces of molecular structures (and others) through the inclusion of the revised Vydrovvan Voorhis nonlocal correlation (rVV10)[13,14] and used the strongly constrained and appropriately normed (SCAN), (r^{2}SCAN) meta-GGA functional.[15,16]

Table S3: The Different Levels of Theory Employed and the Properties Computed in this Study ($\surd$ stands for done, and x for undone).

Functionals	**USPEX searches**	**Structural optimization**	**Single point energy**	**Electronic properties**	**Dynamical stability**
PBE	$\surd$	$\surd$	$\surd$	$\surd$	$\surd$
SCAN+rVV10	x	$\surd$	$\surd$	x	x
r^2SCAN+rVV10	x	$\surd$	$\surd$	x	x
HSE06	x	x	x	$\surd$	x

S1.5 Phonon Dispersion Curves Calculations

In this work, first-principles phonon calculations using the finite displacements method at a quasi-harmonic level are done using the open source package PHONOPY[17,18] (https://github.com/phonopy/phonopy). Supercell structures with displacements are created from a reference unit cell considering all possible crystal symmetry operations. In general, a supercell with cell parameters a, b and c higher than 10 Å is sufficient, but larger ones can be required to avoid unphysical imaginary frequencies, specially at 0 GPa. Force constants are calculated using the optimized structure (VASP) at the PBE level of theory. In the table S4 is given the supercell used for the phonon dispersion curves calculation of each Ga_xS_y phase.

Table S4: Supercell Size Used for the Phonon Calculations of each Ga_xS_y Phase at a Given Pressure.

Ga_xS_y	Pressure (GPa)	Space Group	Supercell size
Ga_2S	20	$I4_1/amd$	1x2x1
GaS	0	$P6_3/mmc$	1x4x4
	10	$C2/m$	3x3x2
	60	R-$3m$	3x4x2
Ga_3S_4	0	$C2/m$	1x2x2
	10	$C2/m$	1x3x2
	40	R-$3m$	2x2x2
Ga_2S_3	0	Cc	2x2x2
	10	$R3m$	1x2x1
	60	R-$3m$	2x2x1
GaS_2	0	$C2/m$	1x1x3
	10	$C2/m$	2x2x2
	60	$Cmcm$	2x2x2

S1.6 *Ab initio* Molecular Dynamics (AIMD) Simulations

Ab initio molecular dynamics (AIMD) within canonical NVT ensemble using the Nosé heat bath scheme were performed to evaluate the thermal stability of specific phases up to 1000 K for 10 ps with a time step of 2 fs, and we allowed 2 ps for thermalization and then extracted data from the last 8 ps. In such AIMD simulations, the Brillouin zone integration is restricted to the Γ point of the supercell, due to a high calculation cost.

S1.7 Mechanical Properties

A fundamental requirement for the viability of a crystal lattice is its mechanical stability under arbitrary small homogeneous deformations. The elastic stability criteria for bulk cubic crystals and various other crystal systems were extensively established by Born and colleagues.[19–21] In VASP, the elastic constants can be calculated using the energy-strain method by setting IBRION = 2 and ISIF = 2, which apply small strains to the equilibrium lattice. The elastic tensor is obtained by evaluating the second derivative of the total energy with respect to these applied strains. For an orthorhombic crystal, the stiffness matrix consists of nine independent elastic constants (C_{11}, C_{12}, C_{13}, C_{22}, C_{23}, C_{33}, C_{44}, C_{55}, C_{66}) with no inherent symmetry relations among them. The necessary and sufficient Born stability criteria for an orthorhombic system are as follows:

$C_{11} > 0$, $C_{11}C_{22} > C_{12}\ C_{12}$,

$C_{11}C_{22}C_{33} + 2C_{12}C_{13}C_{23} - C_{11}C_{23}C_{23} - C_{22}C_{13}\ C_{13} - C_{33}C_{12}C_{12} > 0$,

$C_{44} > 0$, $C_{55} > 0$, $C_{66} > 0$.

Monoclinic and triclinic crystal systems have 13 and 21 independent elastic constants, respectively. The necessary and sufficient Born criteria for monoclinic and triclinic systems:

K3=det$|C_{ij}|$, i,j < 6, K3 >0.

S1.8 Chemical Bonding Analysis, Electronic Band Structures and Band Gap Evaluation

To perform chemical bonding analysis, we carried out for each investigated phase an accurate single-point energy calculation at the GGA-PBE level using the optimized geometry obtained from VASP to calculate the Electron Localization Function (ELF)[22] and plots were managed using VESTA.[23] GGA-PBE functional has proven to be accurate for the description of structural properties of materials. In contrast, it may underestimate the value of the band gap. Therefore, we calculate the band gap (E_g), the Density of States (DOS) and the electronic band structure at the Heyd-Scuseria-Ernzerhof (HSE06)[24] hybrid functional level of theory, using the optimized GGA-PBE structure (single-point energy calculation). This level of theory is noted thereafter as HSE06//PBE. To complement this analysis, we additionally computed the Crystal Orbital Bond Index (COBI),[25] using LOBSTER 5.0.0 package.[26,27] COBI analysis allows the characterization of bonding between two atoms (covalent, metallic, ionic...).

S2 Structural Parameters

Table S5: Structural Parameters of the Predicted Ga_xS_y Phases (distances in Å, angles in °) at the PBE Level of Theory

Phases	P (GPa)	Space Group	Z	Lattice parameters	Atomic coordinates (fractional)
Ga_2S	40	$I4_1/amd$ (SG 141)	4	a=4.654, b=4.654, c=7.365 α=90.0 β=90.0 γ=90.0	Ga 8e(0.000,0.250,0.047); S 4b(0.000,0.250,0.375)
GaS	0	$P6_3/mmc$ (SG 194)	4	a=3.628, b=3.628, c=17.588 α=90.0 β=90.0 γ=120.0	Ga 4f(0.333,0.667,0.320); S 4f(0.333,0.667,0.882)
GaS	10	$C2/m$ (SG 12)	4	a=10.294, b=3.603, c=3.945 α=90.0 β=110.5 γ=90.0	Ga 4i(0.386,0.000,0.025); S 4i(0.846,0.000,0.361)
GaS	60	R-3m (SG 166)	3	a=3.542, b=3.542, c=6.77 α=90.0 β=90.0 γ=120.0	Ga 3a(0.000,0.000,0.000); S 3b(0.000,0.000,0.500)
Ga_3S_4	0	$C2/m$ (SG 12)	2	a=12.071, b=3.589, c=6.24 α=90.0 β=99.7 γ=90.0	Ga 4i(0.263,0.000,0.746), 2a(0.000,0.000,0.000); S 4i(0.627,0.000,0.885), 4i(0.132,0.000,0.376)
Ga_3S_4	10	R-3m (SG 166)	3	a=3.495, b=3.495, c=33.037 α=90.0 β=90.0 γ=120.0	S 6c(0.000,0.000,0.871), 6c(0.000,0.000,0.291); Ga 3a(0.000,0.000,0.000), 6c(0.000,0.000,0.428)
Ga_3S_4	20	$C2/m$ (SG 12)	2	a=11.141, b=3.39, c=5.752 α=90.0 β=98.8 γ=90.0	Ga 4i(0.268,0.000,0.745), 2a(0.000,0.000,0.000); S 4i(0.625,0.000,0.865), 4i(0.117,0.000,0.390)
Ga_2S_3	0	Cc (SG 9)	4	a=11.427, b=6.545, c=7.122 α=90.0 β=121.1 γ=90.0	Ga 4a(0.703,0.435,0.620), 4a(0.044,0.402,0.630); S 4a(0.340,0.086,0.503), 4a(0.672,0.089,0.513), 4a(0.502,0.408,-0.017)
Ga_2S_3	10	$R3m$ (SG 160)	3	a=3.516, b=3.516, c=24.906 α=90.0 β=90.0 γ=120.0	Ga 3a(0.000,0.000,0.840), 3a(0.000,0.000,0.653); S 3a(0.000,0.000,0.132), 3a(0.000,0.000,0.367), 3a(0.000,0.000,-0.072)
Ga_2S_3	10	R-3m (SG 166)	3	a=3.469, b=3.469, c=24.021 α=90.0 β=90.0 γ=120.0	Ga 6c(0.000,0.000,0.402); S 6c(0.000,0.000,0.217), 3a(0.000,0.000,0.000)
GaS_2	0	$C2/m$ (SG 12)	4	a=13.618, b=3.515, c=5.922 α=90.0 β=102.2 γ=90.0	Ga 4i(0.179,0.000,0.616); S 4i(0.800,0.000,0.767), 4i(0.556,0.000,0.652)
GaS_2	20	$C2/m$ (SG 12)	4	a=11.704, b=3.352, c=4.746 α=90.0 β=96.9 γ=90.0	Ga 4i(0.171,0.000,0.723); S 4i(0.816,0.000,0.771), 4i(0.526,0.000,0.713)
GaS_2	40	$Cmcm$ (SG 63)	4	a=3.305, b=10.763, c=4.55 α=90.0 β=90.0 γ=90.0	Ga 4c(0.000,0.343,0.250); S 4c(0.000,0.690,0.250), 4c(0.000,-0.007,0.250)

Table S6: Structural Parameters of Gallium and Sulfur Phases (distances in Å, angles in °) at the PBE Level of Theory.

Phase	**Pressure (GPa)**	**Space group**	**Lattice parameters**	**Atomic coordinates (fractional)**
Ga[28]	0	*Cmce* SG 64	a=4.504, b=7.762, c=4.641 α=β=γ=90.0	Ga 8*f* (0.000, 0.844, -0.082)
Ga[29]	10	$C222_1$ SG 20	a=8.512, b=5.833, c=34.338 α=β=γ=90.0	Ga 4*a* (0.688, 0.000, 0.000), Ga 8*c* (-0.031, 0.195, -0.021), Ga 8*c* (0.283, 0.078, -0.036), Ga 8*c* (0.562, 0.279, -0.058), Ga 8*c* (0.278, 0.469, -0.079), Ga 8*c* (-0.036, 0.352, -0.094), Ga 8*c* (0.189, 0.059, 0.884), Ga 8*c* (0.477, 0.244, 0.864), Ga 8*c* (0.790, 0.123, 0.849), Ga 8*c* (0.059, 0.341, 0.827), Ga 8*c* (0.256, 0.015, 0.807), Ga 4*b* (0.000, 0.727, 0.250), Ga 8*c* (0.305, 0.119, 0.732), Ga 8*c* (0.547, 0.382, 0.709)
Ga[30]	20	$I4/mmm$ SG 139	a=2.647, b=2.647, c=4.285 α=β=γ=90.0	Ga 2*a* (0.000, 0.000, 0.000)
S[31]	0	*Fddd* SG 70	a=12.190, b=14.615, c=25.591 α=β=γ=90.0	S 32*h* (0.141, 0.194, 0.206), S 32*h* (0.270, 0.221, 0.256), S 32*h* (0.208, 0.263, 0.327), S 32*h* (0.203, 0.153, 0.378)
S[32]	10	*R*-3 SG 148	a=b=9.988, c=3.666 α=β=90.0, γ=120.0	S 18*f* (0.160, 0.203, 0.125)
S[33]	55	$I4_1/acd$ SG 142	a=b=7.866, c= 3.123 α=β=γ=90.0	S 16*f* (0.131, 0.381, 0.125)
S	100	*R*-3*m* SG 166	a=b=3.495, c=2.834 α=γ=90.0, β=120.0	S 3*a* (0.000, 0.000, 0.000)

S3 Energies

Table S7: Calculated Enthalpies of the Predicted Ga_xS_y Compounds at the PBE Level of Theory.

Structure	**Space group**	**Pressure (GPa)**	**Enthalpy (eV/atom)**	**ZPE (eV/atom)**	**Formation Enthalpy (eV/atom)**
Ga_2S	$I4_1/amd$ SG 141	40	0.247	0.034	-0.371
GaS	$P6_3/mmc$ SG 194	0	-4.165	0.038	-0.651
GaS	$C2/m$ SG 12	10	-2.888	0.040	-0.604
GaS	R-3m SG 166	60	1.555	0.050	-0.476
Ga_3S_4	R-3m SG 166	10	-3.005	0.039	-0.652
Ga_3S_4	$C2/m$ SG 12	20	-1.991	0.038	-0.639
Ga_2S_3	Cc SG 9	0	-4.297	0.040	-0.661
Ga_2S_3	$R3m$ SG 160	10	-3.037	0.044	-0.656
Ga_2S_3	R-3m SG 166	10	-3.022	0.056	-0.642
GaS_2	$C2/m$ SG 12	20	-1.990	0.043	-0.549
GaS_2	$Cmcm$ SG 63	40	-0.191	0.056	-0.491
Quenchable					
Ga_3S_4	$C2/m$ SG 12	0	-4.091	0.039	-0.488
GaS_2	$C2/m$ SG 12	0	-4.141	0.032	-0.422

Table S8: Calculated Enthalpies of the Gallium and Sulfur Phases at the PBE, SCAN+rVV10, and r^{2}SCAN+rVV10 Levels of Theory.

Phase	**Pressure (GPa)**	**Space group**	**ZPE (eV/atom)**	**Enthalpy (eV/atom)**		
				PBE	**SCAN+ rVV10**	**r^2SCAN+ rVV10**
Ga	0	$Cmce$ SG 64	0.022	-2.904	-16.071	-11.0356
Ga	10	$C222_1$ SG 20	0.023	-1.802	-14.977	-9.924
Ga	40	$I4/mmm$ SG 139	0.037	0.936	-12.359	-7.26525
S	0	$Fddd$ SG 70	0.040	-4.124	-9.514	-7.865
S	10	R-3 SG 148	0.048	-2.766	-8.286	-6.627
S	40	$I4_1/acd$ SG 142	0.060	-0.018	-5.530	-3.868
S	100	R-3$/m$ SG 166	0.060	4.186	-1.210	0.438

Table S9: Calculated Enthalpies of the Predicted Ga_xS_y Compounds at the SCAN+rVV10 and r^{2}SCAN+rVV10 Levels of Theory.

Structure	**Space group**	**Pressure (GPa)**	**Enthalpy (eV/atom)**		**Formation Enthalpy (eV/atom)**	
			SCAN+ rVV10	**r^2SCAN+ rVV10**	**SCAN+ rVV10**	**r^2SCAN+ rVV10**
Ga_2S	$I4_1/amd$ SG 141	40	-10.448	-6.573	-0.365	-0.440
GaS	$P6_3/mmc$ SG 194	0	-13.517	-10.218	-0.725	-0.767
GaS	$C2/m$ SG 12	10	-12.291	-8.990	-0.660	-0.715
GaS	R-3m SG 166	60	-7.900	-4.595	-0.497	-0.583
Ga_3S_4	R-3m SG 166	10	-11.852	-8.802	-0.699	-0.762
Ga_3S_4	$C2/m$ SG 12	20	-10.860	-7.809	-0.682	-0.753
Ga_2S_3	Cc SG 9	0	-12.905	-9.941	-0.768	-0.807
Ga_2S_3	$R3m$ SG 160	10	-11.693	-8.732	-0.731	-0.786
Ga_2S_3	R-3m SG 166	10	-11.667	-8.711	-0.705	-0.765
GaS_2	$C2/m$ SG 12	20	-10.140	-7.399	-0.608	-0.663
GaS_2	$Cmcm$ SG 63	40	-8.357	-5.612	-0.551	-0.611
Quenchable						
Ga_3S_4	$C2/m$ SG 12	0	-12.899	-9.849	-0.575	-0.626
GaS_2	$C2/m$ SG 12	0	-12.201	-9.463	-0.501	-0.541

S4 Thermodynamic Stability

The pressure-composition phase diagrams of the Ga-S system are computed at 0, 10, 40 and 100 GPa at the PBE, SCAN+rVV10, and r^{2}SCAN+rVV10 levels of theory. The results are shown in the figure S5, and the distance from the hull are given in the table S10.

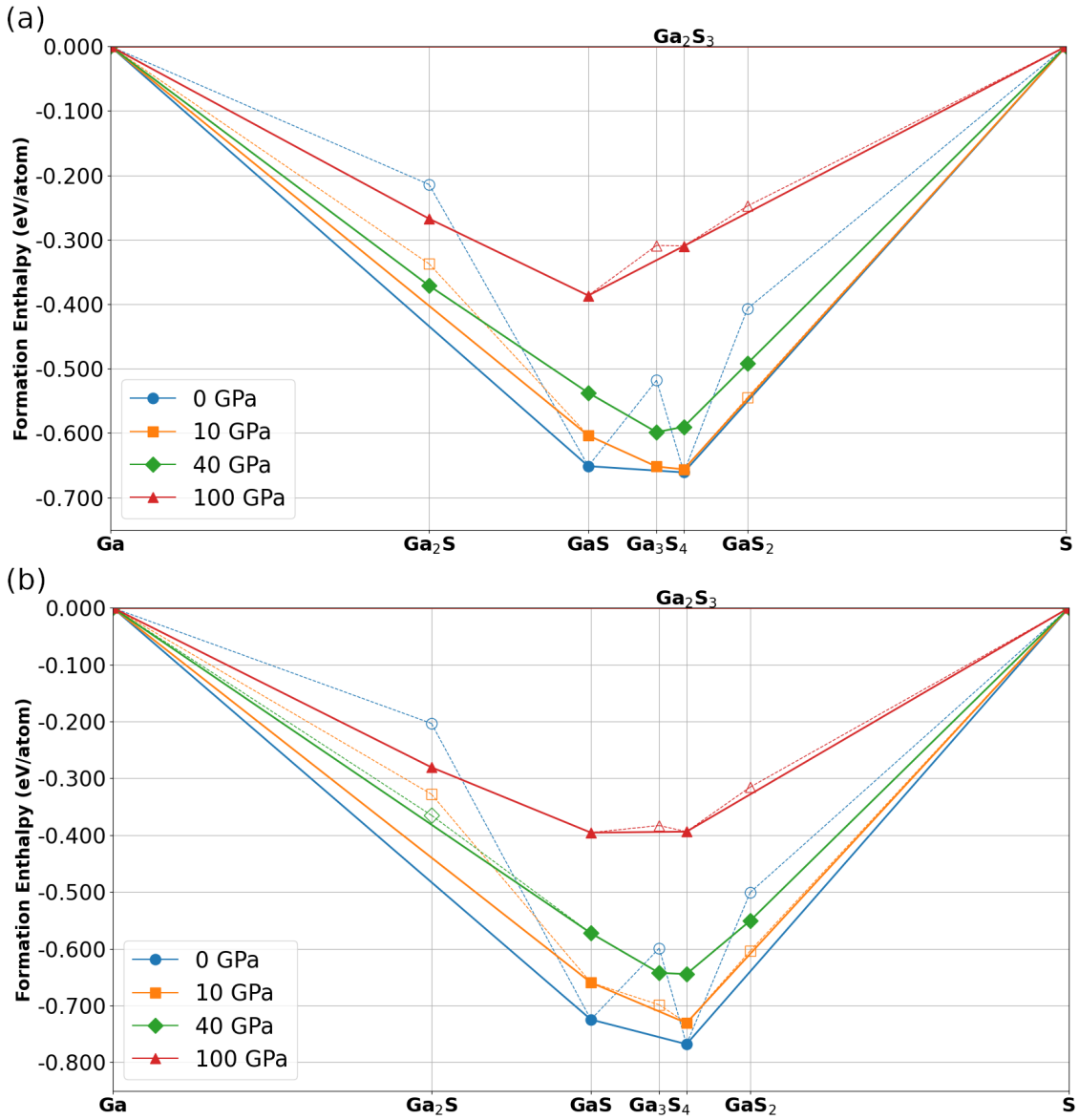

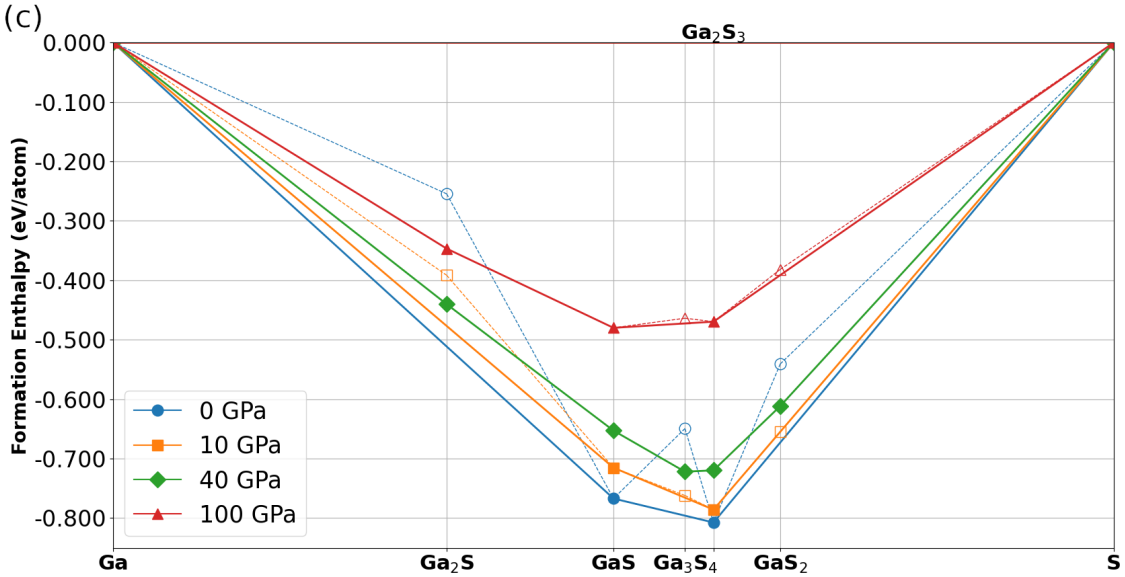

Figure S5: The convex hulls of the Ga-S system at (a) PBE (b) SCAN+rVV10 (c) r^2SCAN+rVV10 levels of theory. Solid symbols denote stable structures, and empty ones represent metastable structures.

Table S10: Distance From the Hull (eV/atom) of the Predicted Ga_xS_y Compounds at the PBE, SCAN and r^{2}SCAN Levels of Theory.

Phases	**Space group**	**Pressure (GPa)**	**Distance from the hull (eV/atom)**		
			PBE	**SCAN+ rVV10**	**r^2SCAN+ rVV10**
Ga_2S	$I4_1/amd$	0	0.220	0.280	0.260
	$I4_1/amd$	10	0.070	0.115	0.090
	$I4_1/amd$	40	0.000	0.016	0.000
	$I4_1/amd$	100	0.000	0.000	0.000
GaS	$P6_3/mmc$	0	0.000	0.000	0.000
	$C2/m$	10	0.000	0.000	0.000
	$C2/m$	40	0.000	0.000	0.000
	R-3m	100	0.000	0.000	0.000
Ga_3S_4	R-3m	0	0.141	0.157	0.147
	R-3m	10	0.000	0.012	0.004
	R-3m	40	0.000	0.000	0.000
	R-3m	100	0.023	0.012	0.009
Ga_3S_4	$C2/m$	0	0.170	0.185	0.175
	$C2/m$	10	0.007	0.035	0.025
	$C2/m$	40	0.000	0.000	0.000
	$C2/m$	100	0.040	0.035	0.030
Ga_2S_3	Cc	0	0.000	0.000	0.000
	$R3m$	10	0.000	0.000	0.000
	R-3m	40	0.000	0.000	0.000
	R-3m	100	0.000	0.000	0.000
GaS_2	$C2/m$	0	0.145	0.140	0.140
	$C2/m$	10	0.003	0.006	0.001
	$C2/m$	40	0.000	0.000	0.000
	$Cmcm$	100	0.008	0.010	0.010

S5 Domain Stability

The relative enthalpy per atom as a function of pressure (H(P) curves) for competing structures is computed to determine the phase transition pressure(s) of a given compound from 0 to 100 GPa. H(P) are given in the following figures at the PBE, SCAN and r^{2}SCAN levels of theory.

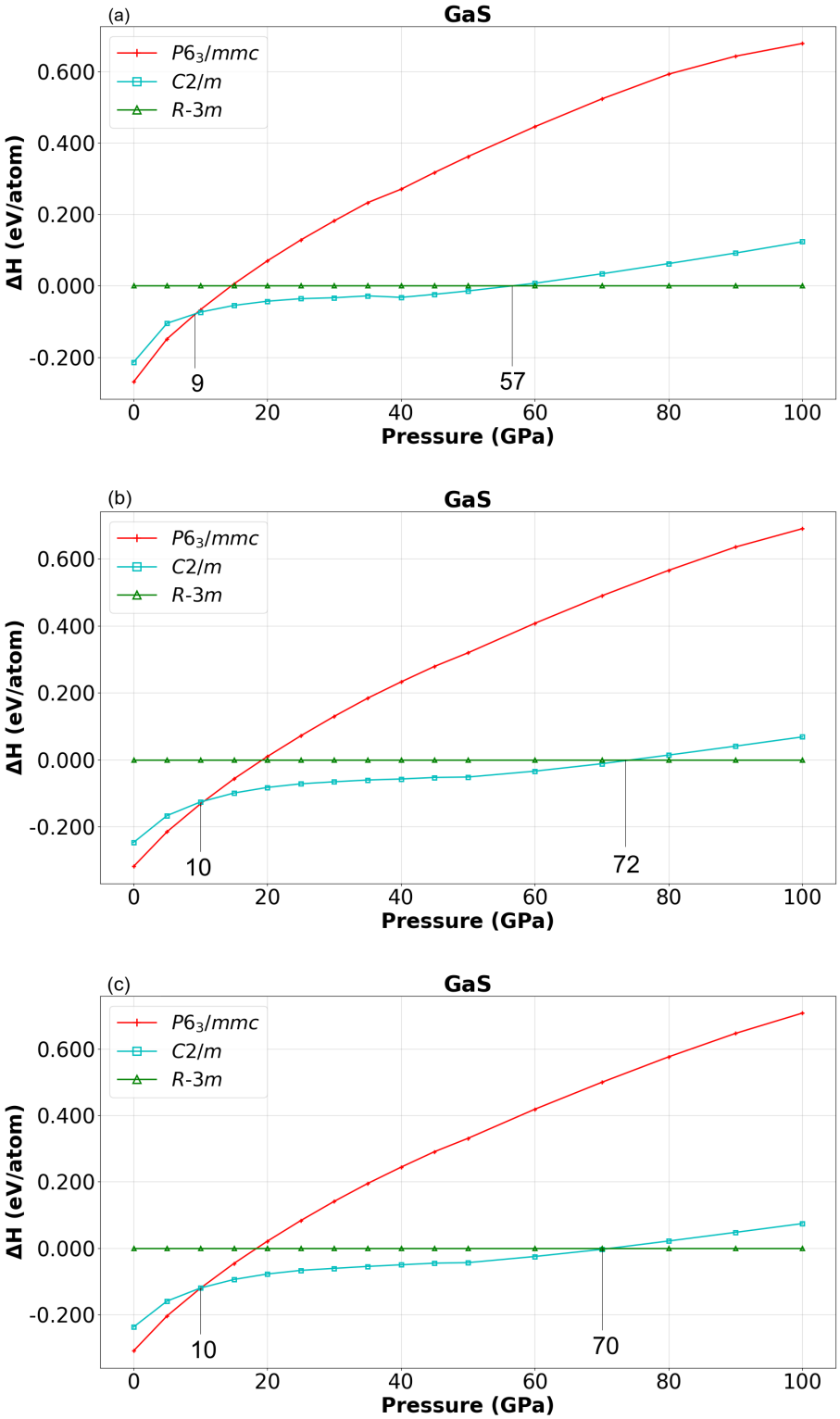

Figure S6: The calculated enthalpy differences of various GaS structures relative to the R-3m structure as a function of pressure at (a) PBE, (b) SCAN+rVV10, and (c) r^{2}SCAN+rVV10 levels of theory.

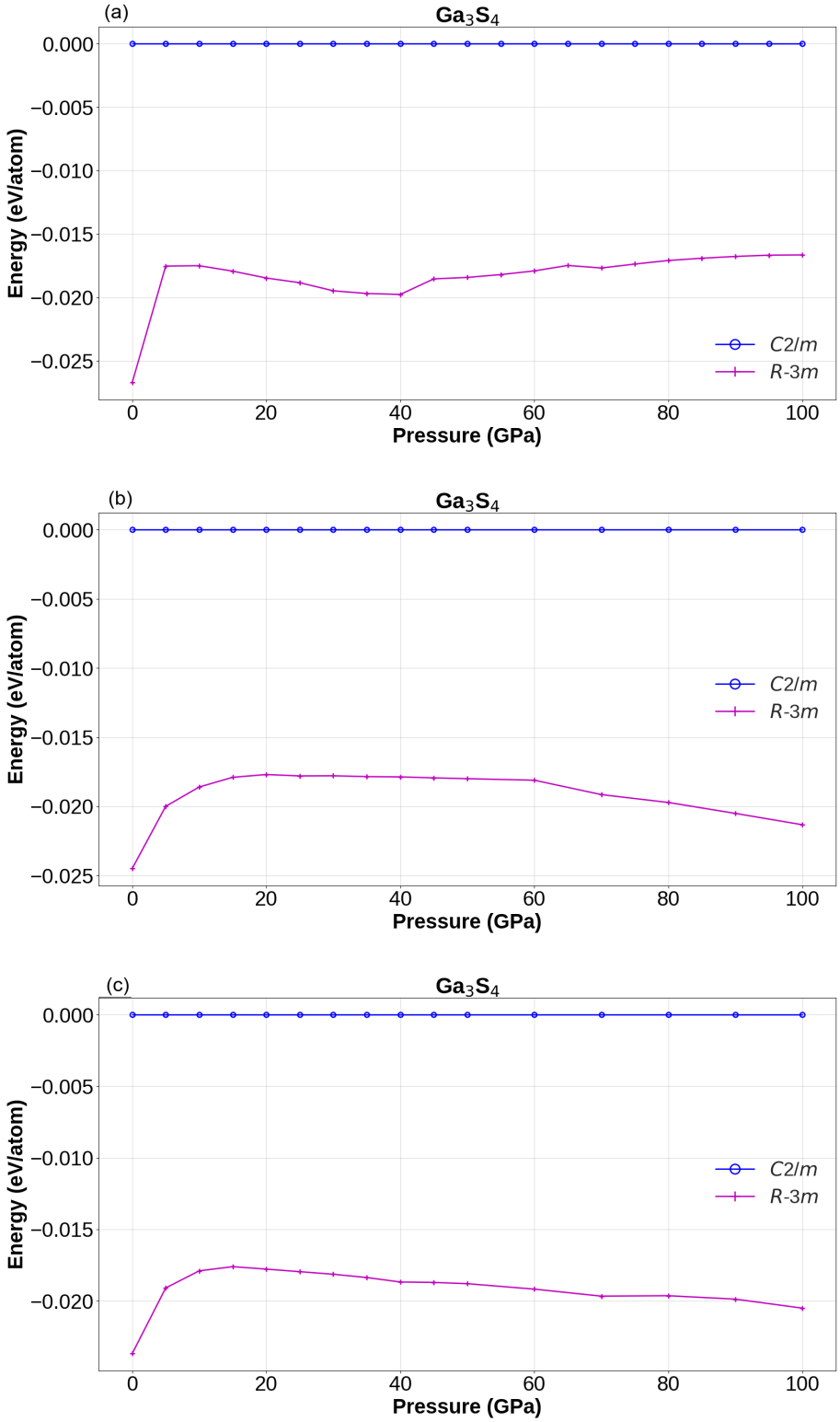

Figure S7: The calculated enthalpy differences of various Ga_3S_4 structures relative to the $C2/m$ structure as a function of pressure at (a) PBE, (b) SCAN+rVV10, and (c) r^2SCAN+rVV10 levels of theory.

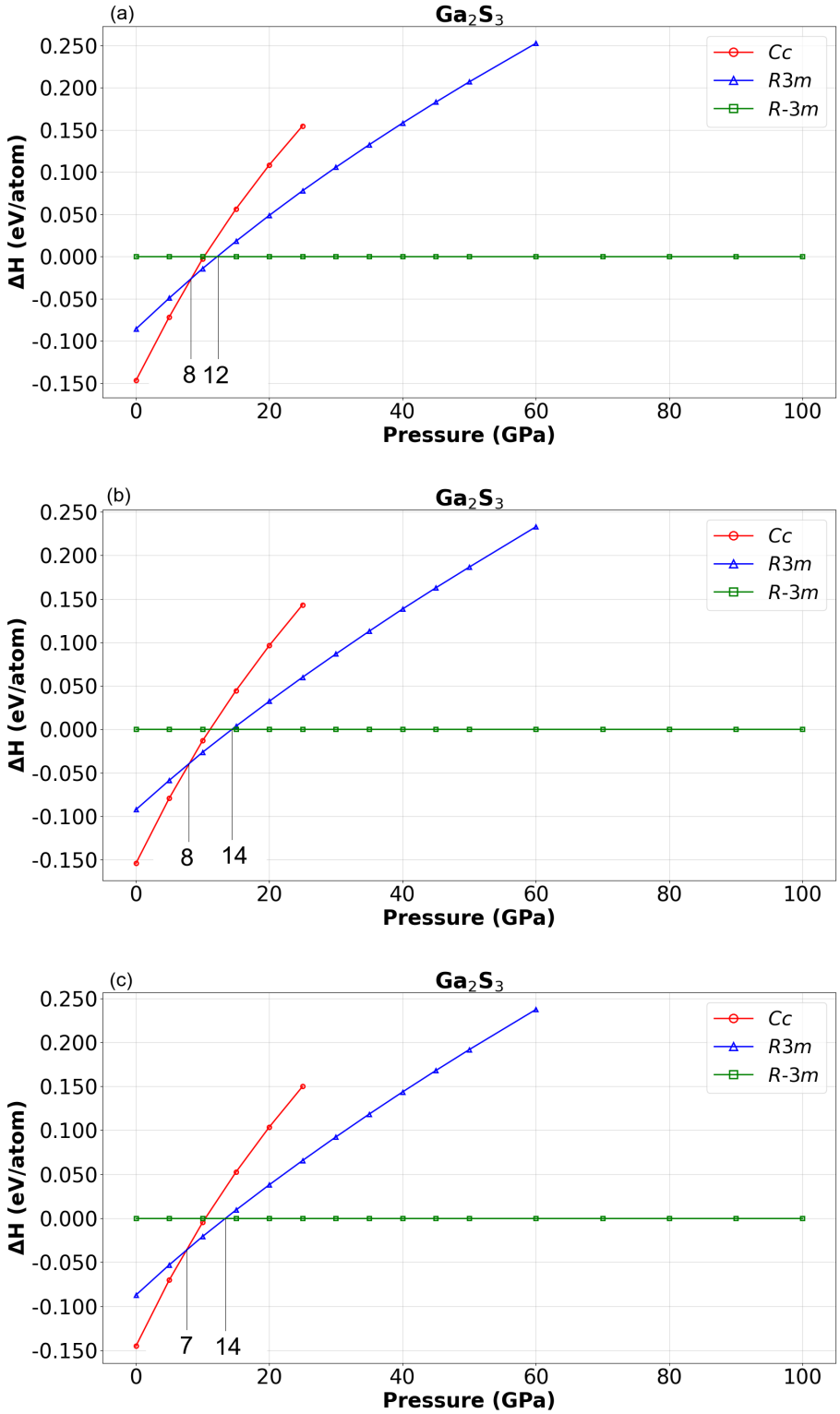

Figure S8: The calculated enthalpy differences of various Ga_2S_3 structures relative to the R-3m structure as a function of pressure at (a) PBE, (b) SCAN+rVV10, and (c) r^{2}SCAN+rVV10 level of theory.

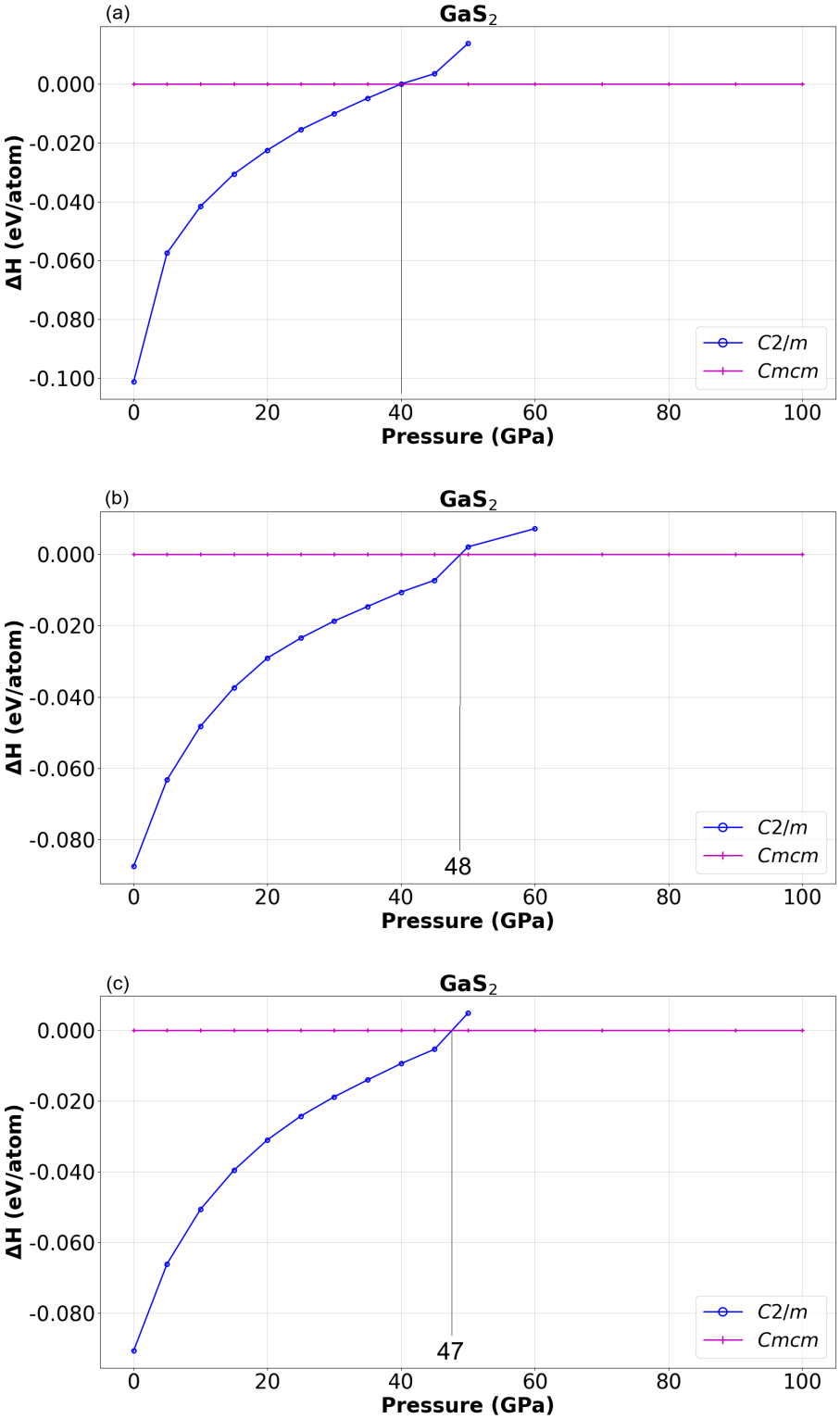

Figure S9: The calculated enthalpy differences of various GaS_2 structures relative to the *Cmcm* structure as a function of pressure at (a) PBE, (b) SCAN+rVV10, and (c) r^2SCAN+rVV10 level of theory.

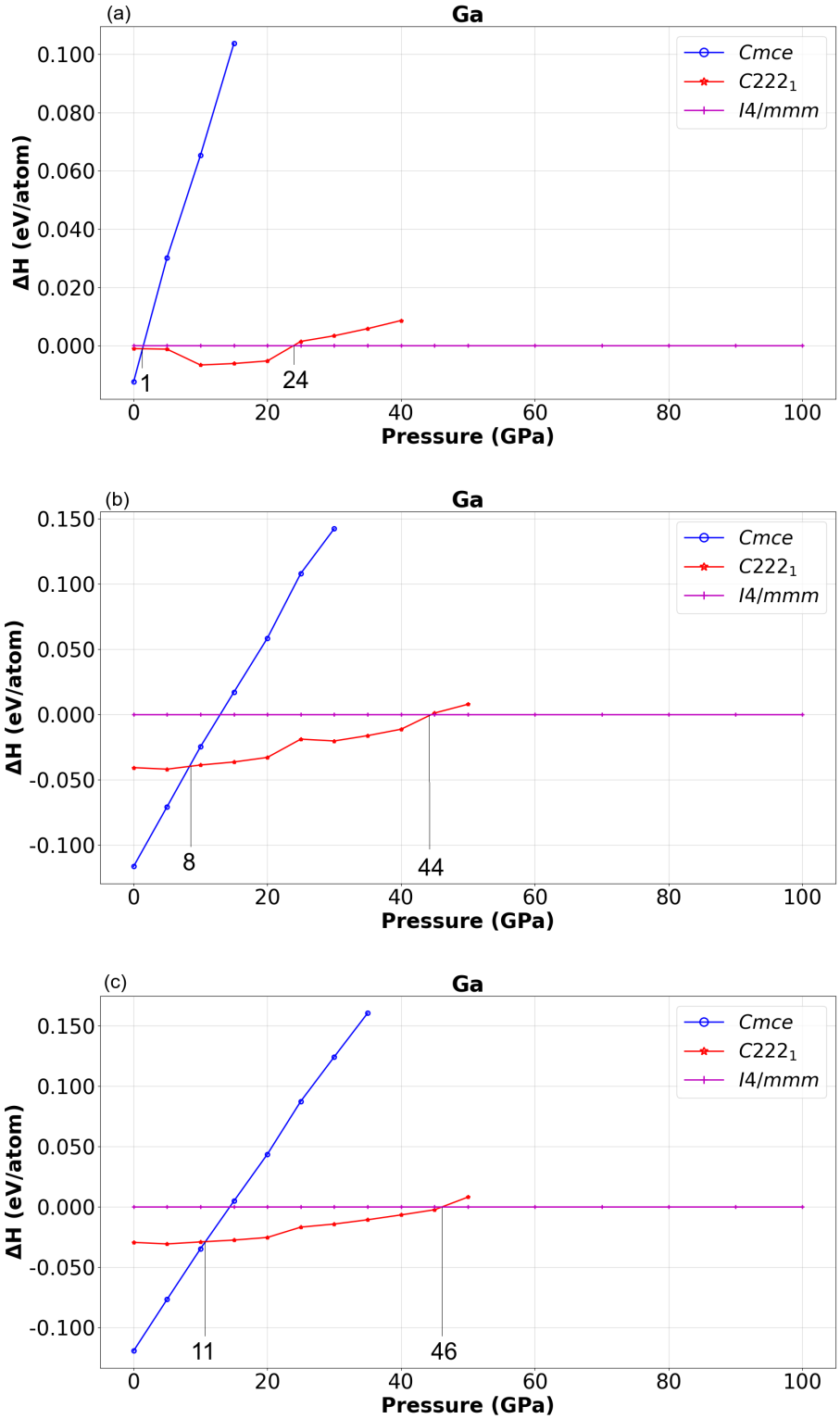

Figure S10: The calculated enthalpy differences of various gallium structures relative to the $I4/mmm$ structure as a function of pressure at (a) PBE, (b) SCAN+rVV10 and (c) r^{2}SCAN+rVV10 level of theory.

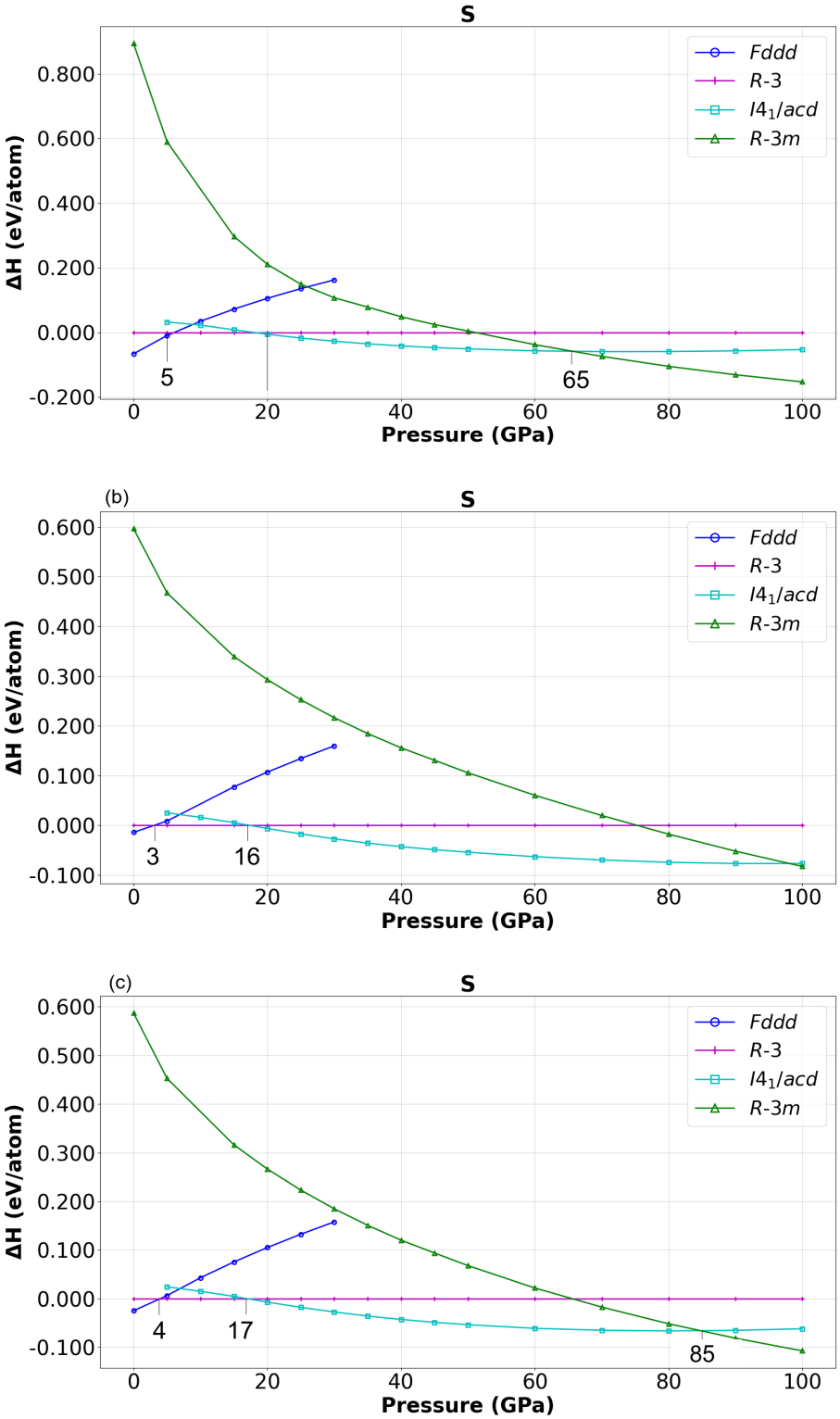

Figure S11: The calculated enthalpy differences of sulfur structures relative to the $C222_1$ structure as a function of pressure at (a) PBE, (b) SCAN+rVV10 and (c) r^{2}SCAN+rVV10 level of theory.

S6 Dynamical Stability

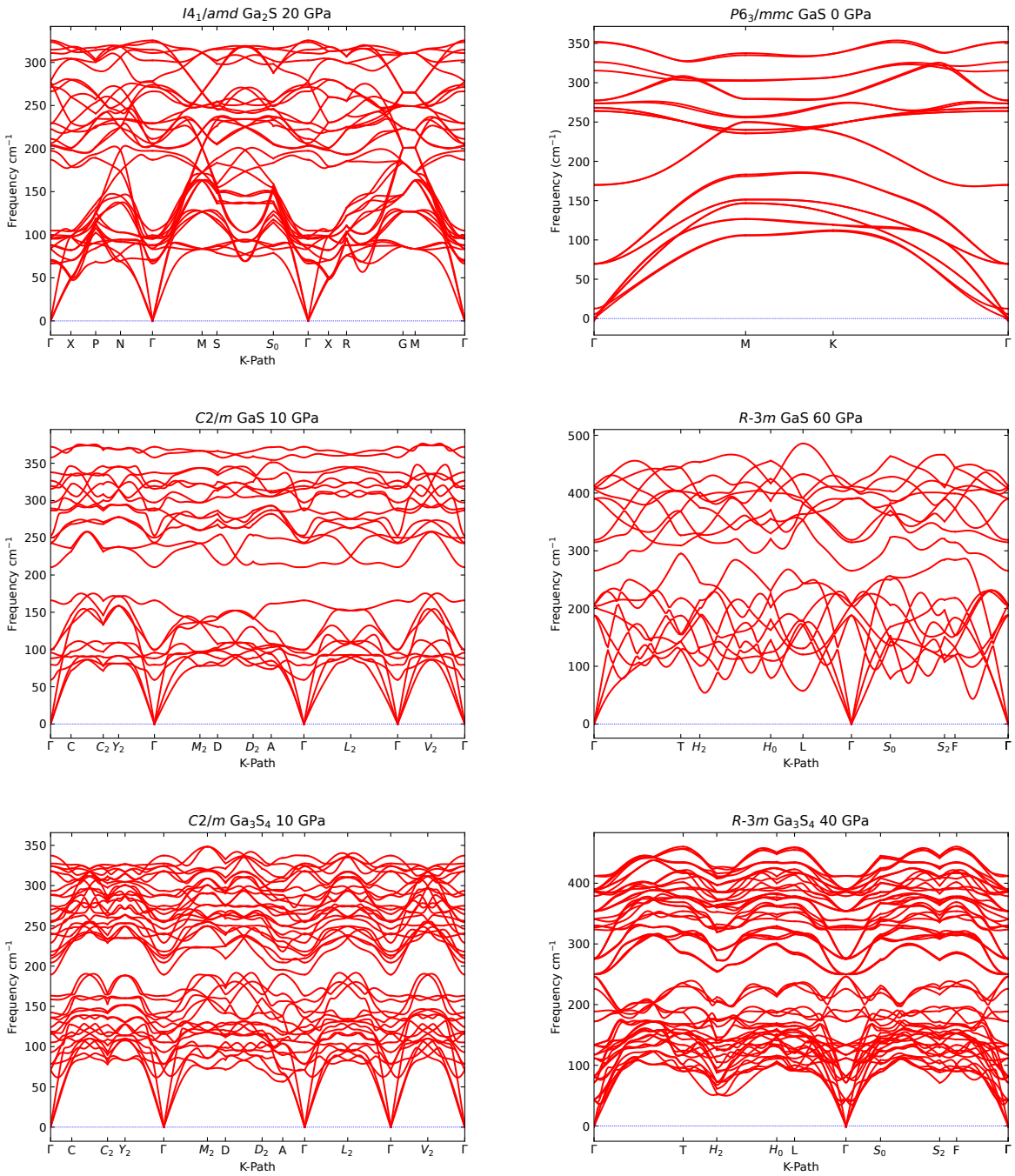

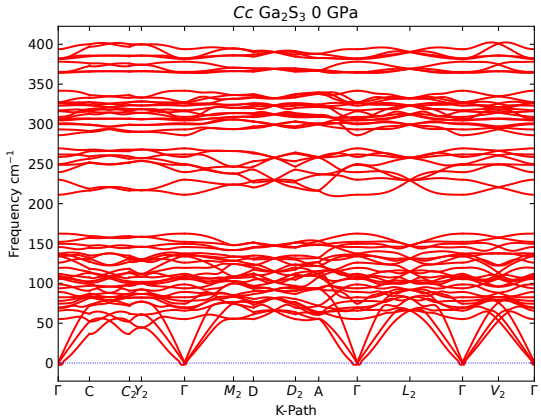
Cc Ga2S3 0 GPa
Frequency cm−1
K-Path
Γ C C2 Y2 Γ M2 D D2 A Γ L2 Γ V2 Γ

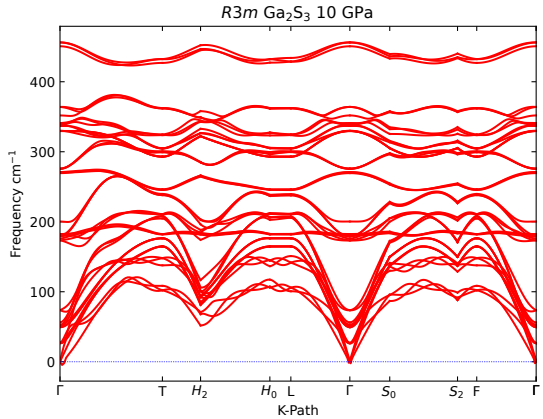
R3m Ga2S3 10 GPa
Frequency cm−1
K-Path
Γ T H2 H0 L Γ S0 S2 F Γ

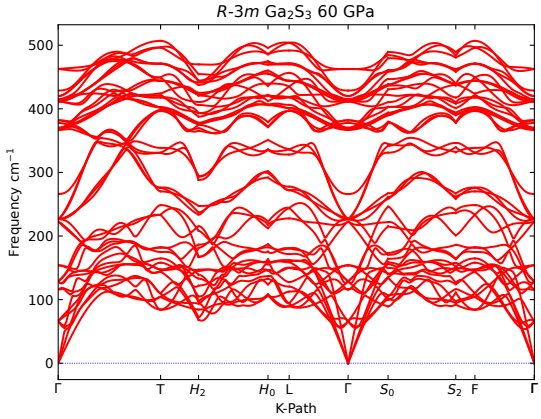
R-3m Ga2S3 60 GPa
Frequency cm−1
K-Path
Γ T H2 H0 L Γ S0 S2 F Γ

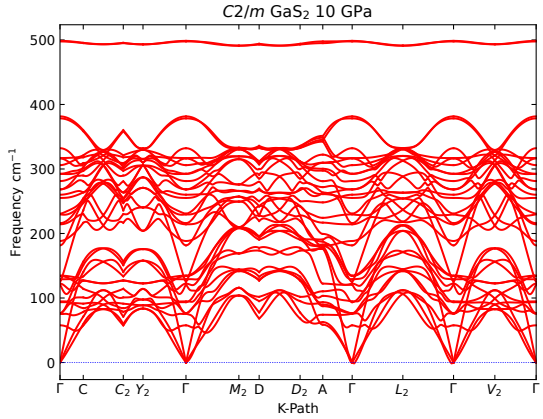
C2/m GaS2 10 GPa
Frequency cm−1
K-Path
Γ C C2 Y2 Γ M2 D D2 A Γ L2 Γ V2 Γ

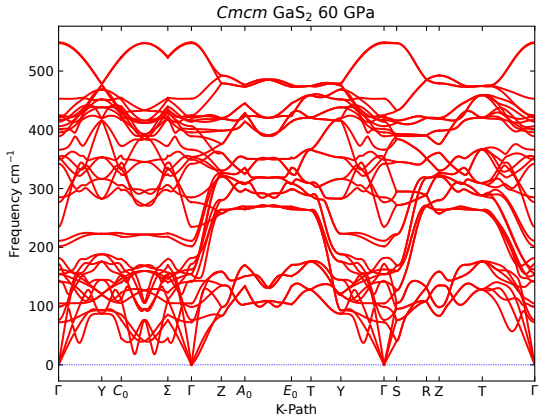
Cmcm GaS2 60 GPa
Frequency cm−1
K-Path
Γ Y C0 Σ Γ Z A0 E0 T Y Γ S R Z T Γ

Quenchable phases

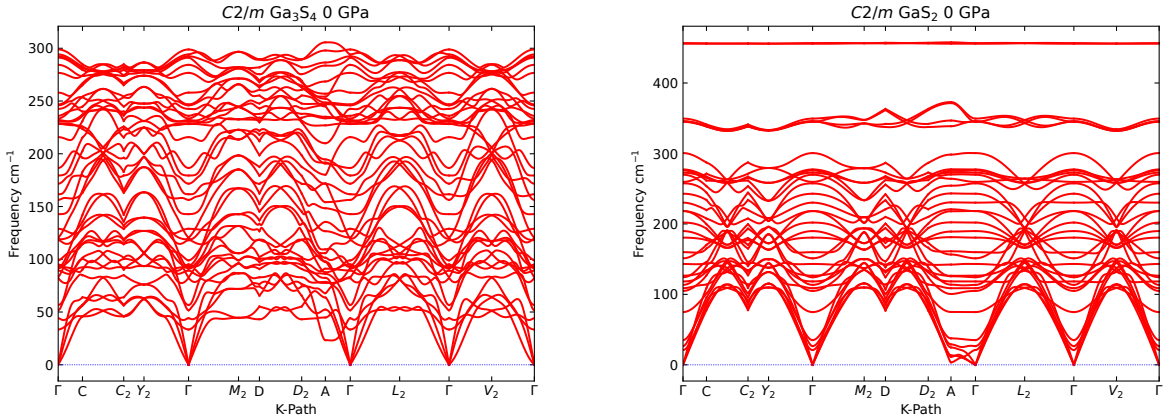

Figure S12: Phonon dispersion curves of Ga_xS_y at a given pressure in GPa (PBE level of theory).

S7 Simulated X-Ray Diffraction Patterns

X-Ray diffraction (XRD) is routinely used to identify crystalline phases and can provide unit cell information. We computed the XRD spectrum of each phase at a given pressure, using λ Cu K-α (1.542 Å). The XRD patterns are presented in Figure S13.

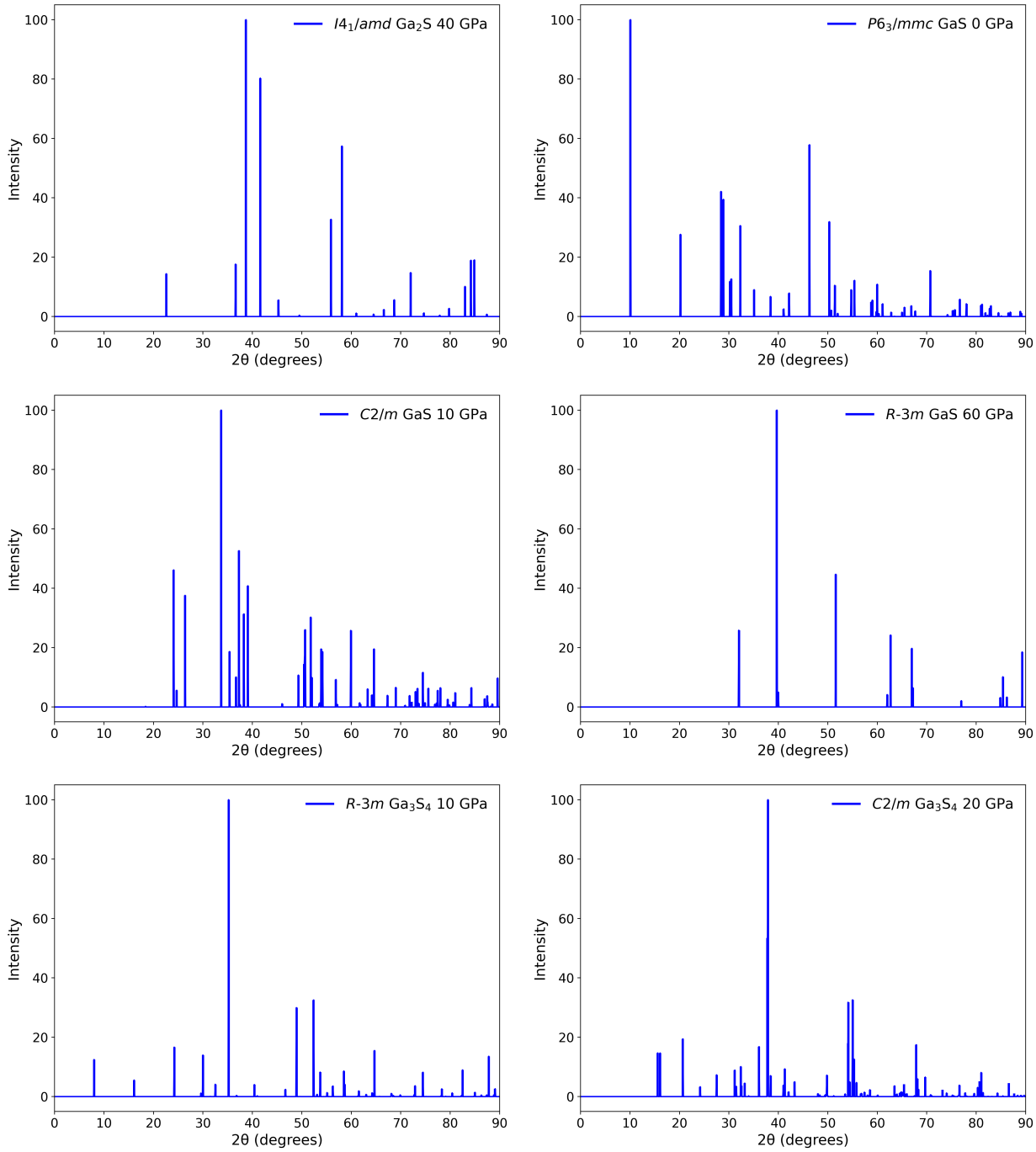
$I4_1/amd$ Ga_2S 40 GPa
$P6_3/mmc$ GaS 0 GPa
$C2/m$ GaS 10 GPa
R-3m GaS 60 GPa
R-3m Ga_3S_4 10 GPa
$C2/m$ Ga_3S_4 20 GPa
Intensity
2θ (degrees)

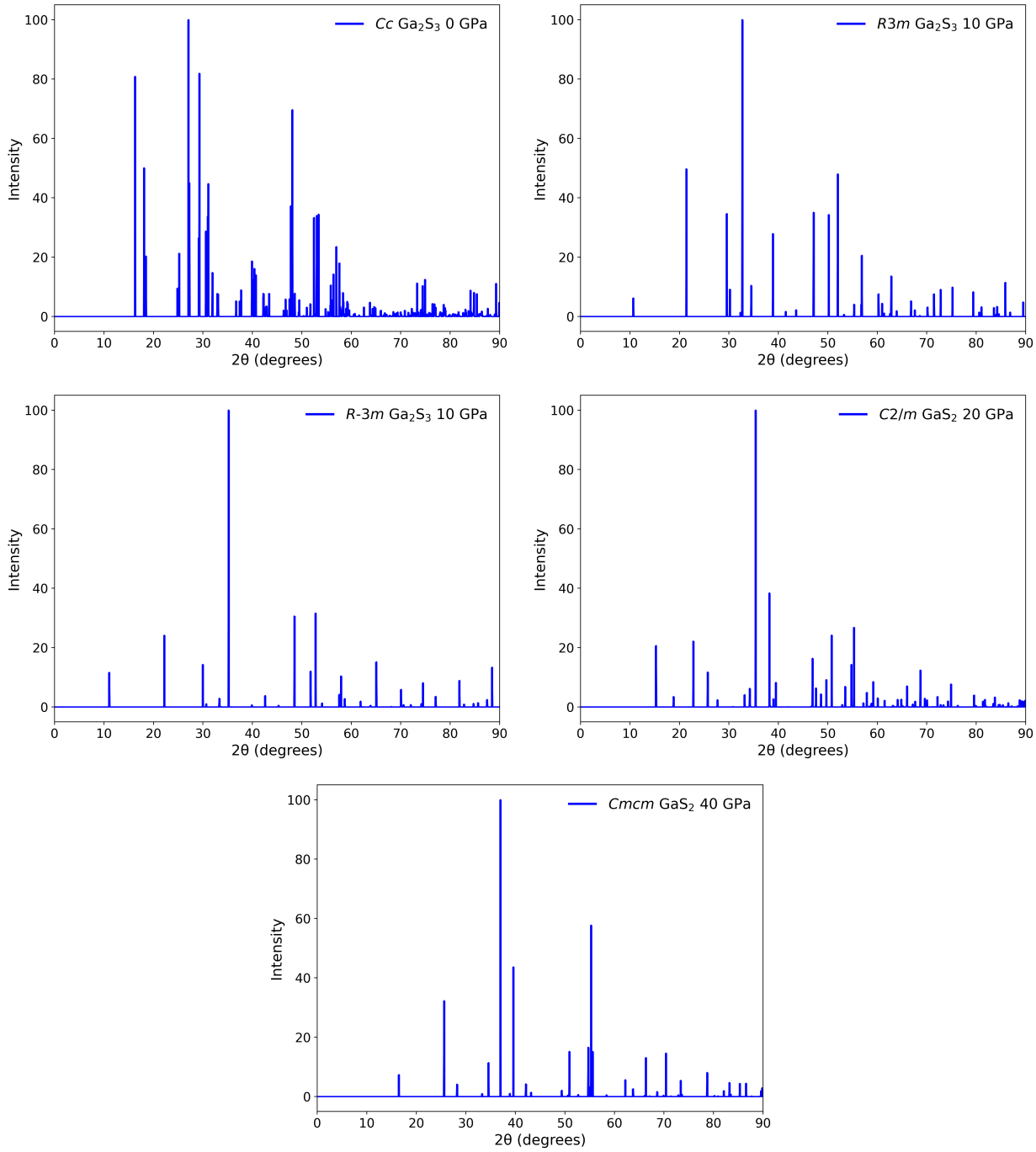

Figure S13: Calculated X-ray diffraction patterns of Ga_xS_y at given pressures in GPa (crystal structures at the PBE level of theory).

S8 Electronic Properties

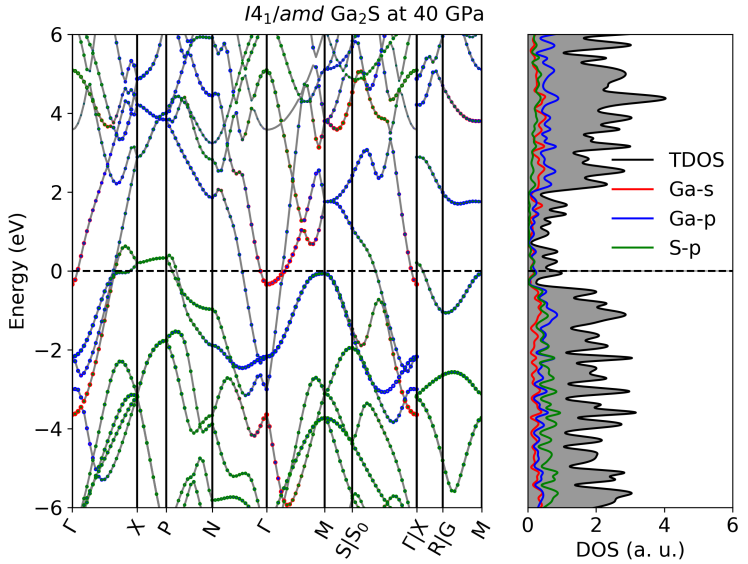

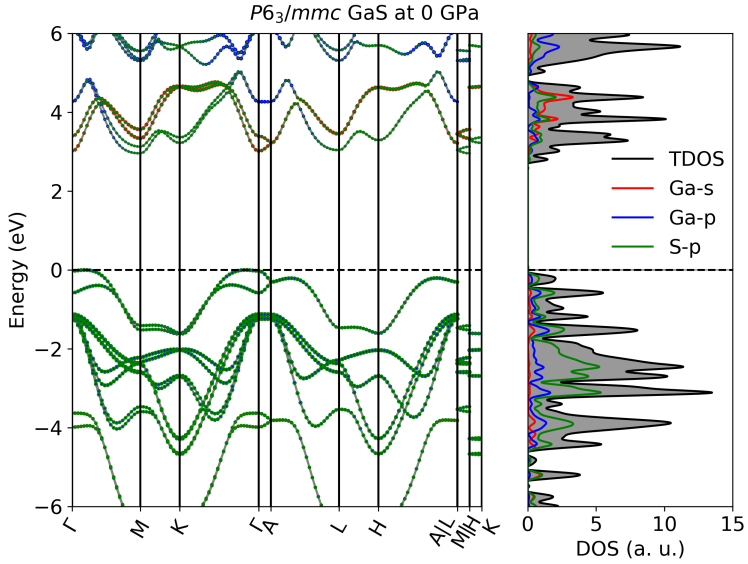

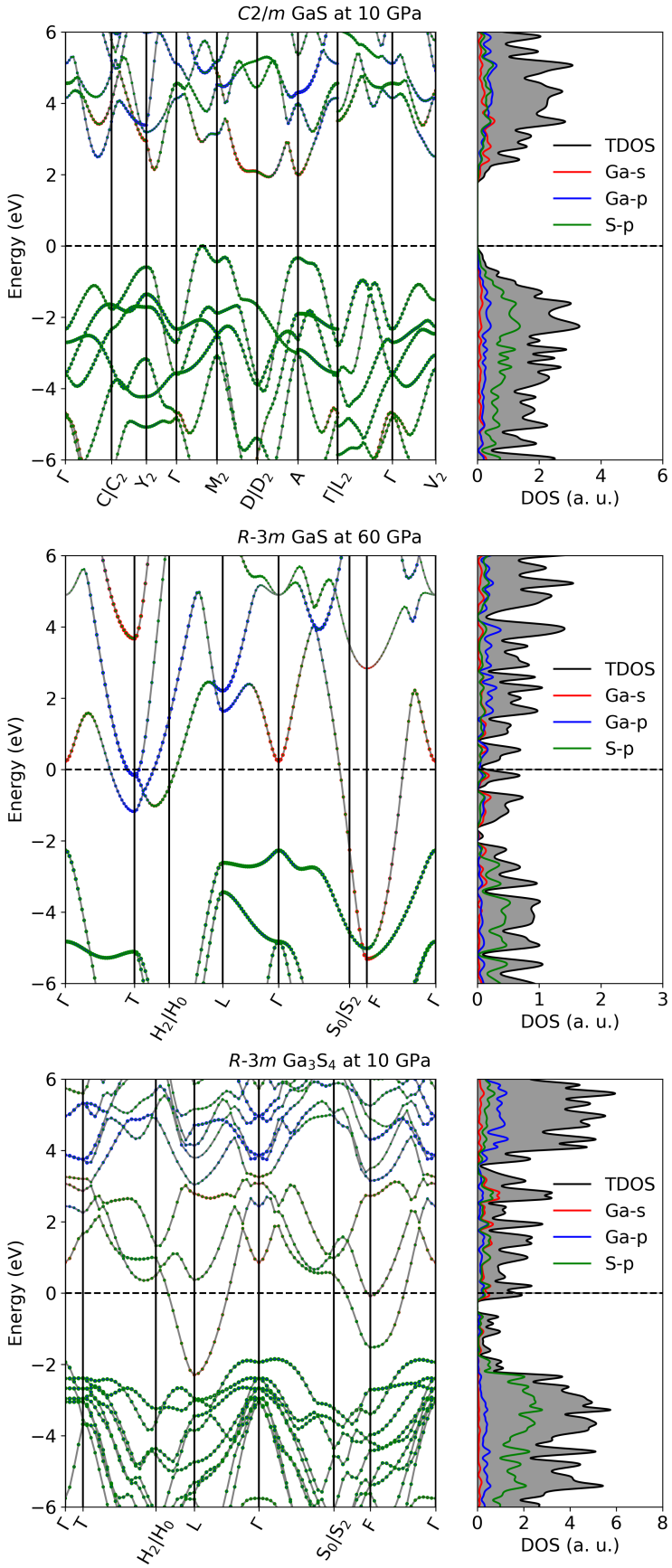
C2/m GaS at 10 GPa
Energy (eV)
Γ
C|C2
Y2
Γ
M2
D|D2
A
Γ|L2
Γ
V2
DOS (a. u.)
TDOS
Ga-s
Ga-p
S-p
R-3m GaS at 60 GPa
Γ
T
H2|H0
L
Γ
S0|S2
F
Γ
R-3m Ga3S4 at 10 GPa

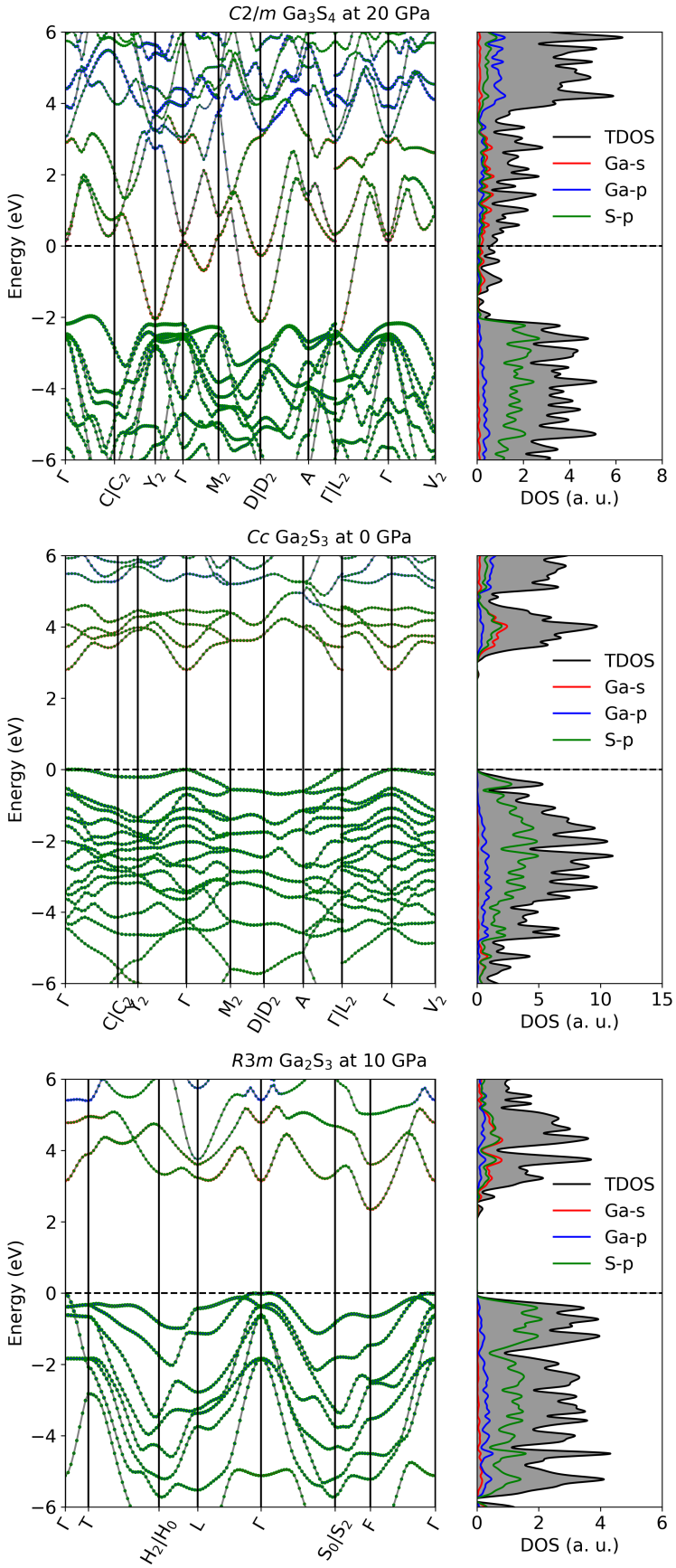
C2/m Ga3S4 at 20 GPa
Energy (eV)
Γ
C|C2
Y2
Γ
M2
D|D2
A
Γ|L2
Γ
V2
DOS (a. u.)
TDOS
Ga-s
Ga-p
S-p
Cc Ga2S3 at 0 GPa
Energy (eV)
Γ
C|C2
Y2
Γ
M2
D|D2
A
Γ|L2
Γ
V2
DOS (a. u.)
TDOS
Ga-s
Ga-p
S-p
R3m Ga2S3 at 10 GPa
Energy (eV)
Γ
T
H2|H0
L
Γ
S0|S2
F
Γ
DOS (a. u.)
TDOS
Ga-s
Ga-p
S-p

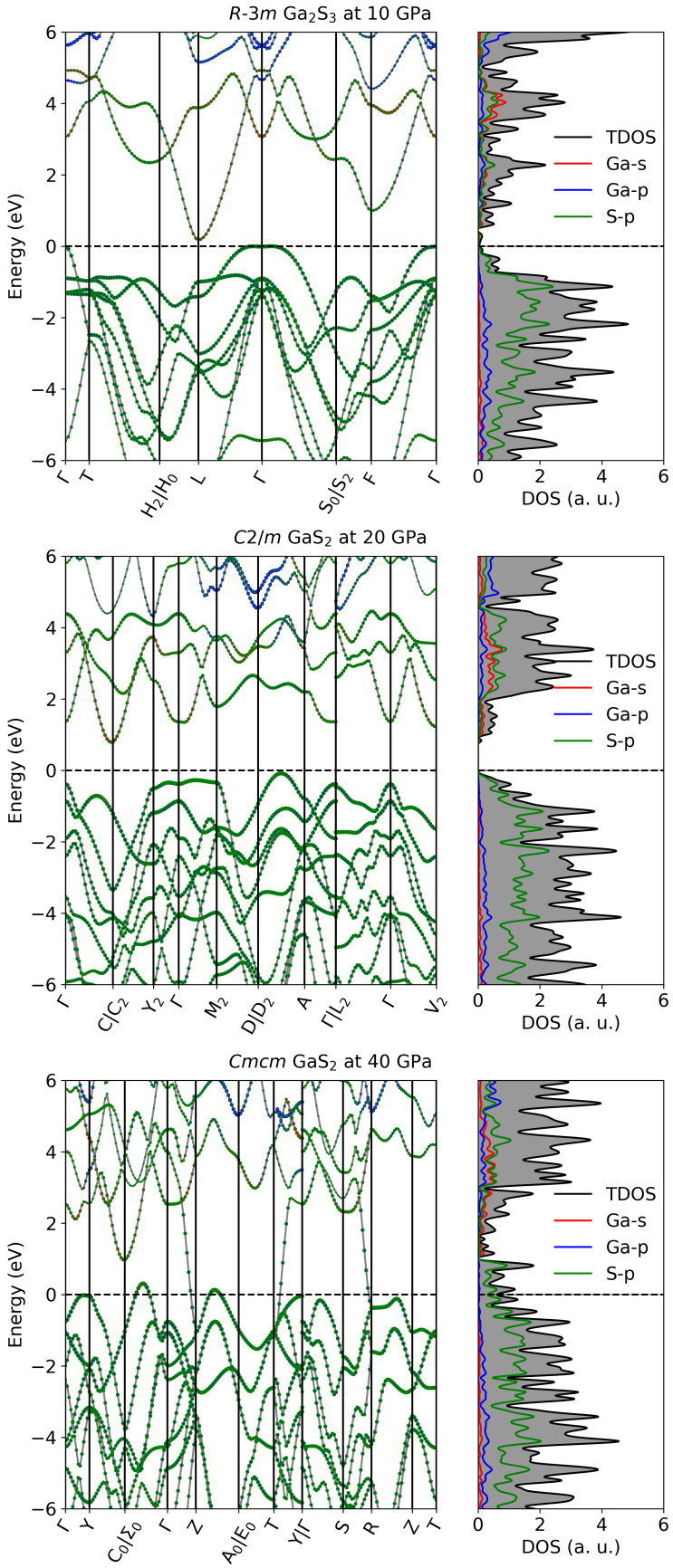
R-3m Ga2S3 at 10 GPa
Energy (eV)
Γ T H2|H0 L Γ S0|S2 F Γ
DOS (a. u.)
TDOS
Ga-s
Ga-p
S-p
C2/m GaS2 at 20 GPa
Energy (eV)
Γ C|C2 Y2 Γ M2 D|D2 A Γ|L2 Γ V2
DOS (a. u.)
TDOS
Ga-s
Ga-p
S-p
Cmcm GaS2 at 40 GPa
Energy (eV)
Γ Y C0|Σ0 Γ Z A0|E0 T Y|Γ S R Z T
DOS (a. u.)
TDOS
Ga-s
Ga-p
S-p

Quenchable phases

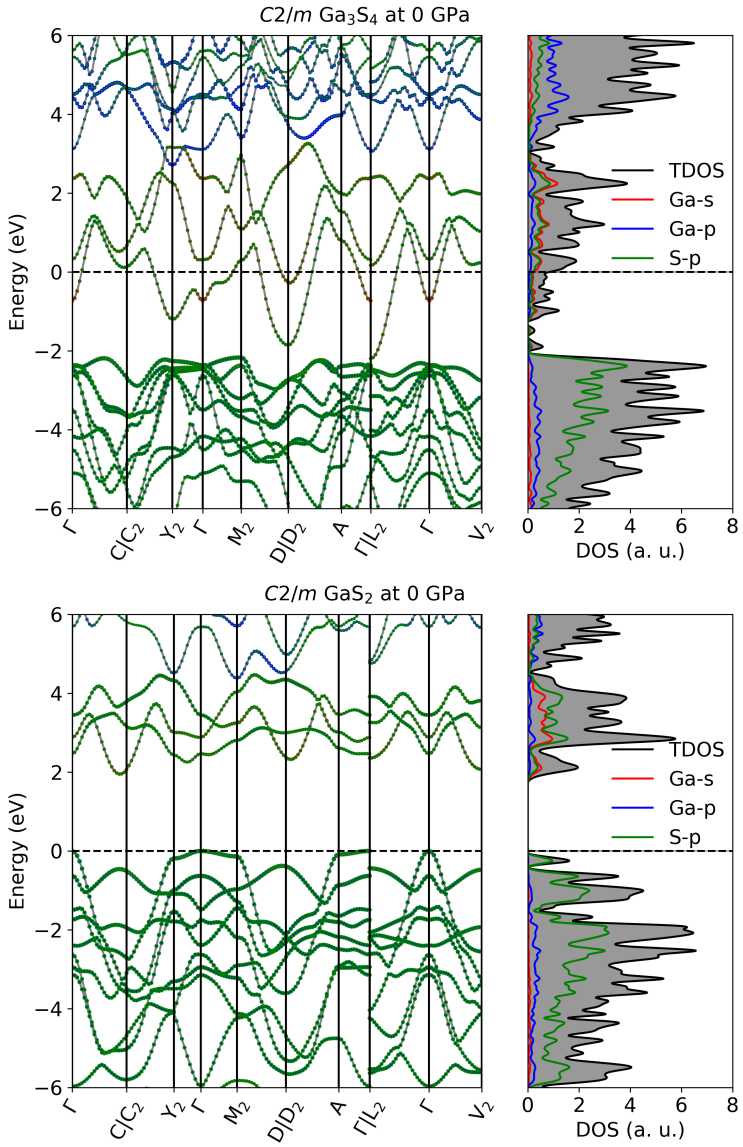

Figure S14: Band structures and DOS of Ga_xS_y at a given pressure (HSE06//PBE level of theory).

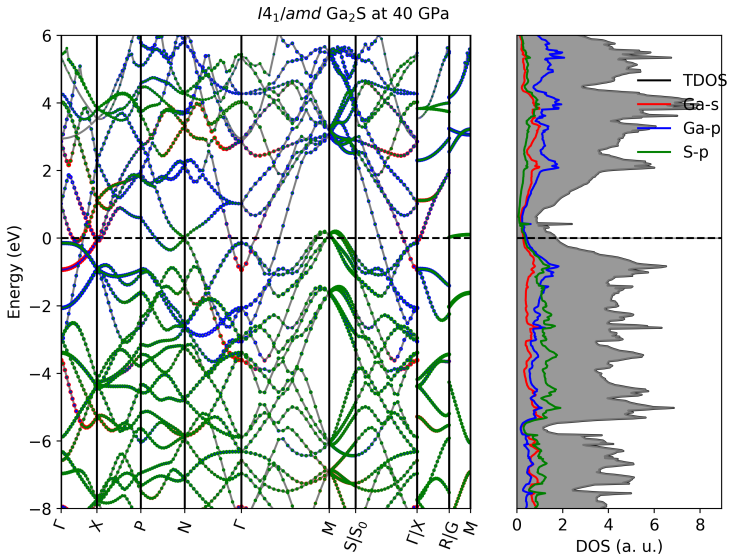
$I4_1/amd$ Ga_2S at 40 GPa
Energy (eV)
Γ
X
P
N
Γ
M
S|S$_0$
Γ|X
R|G
M
DOS (a. u.)
TDOS
Ga-s
Ga-p
S-p

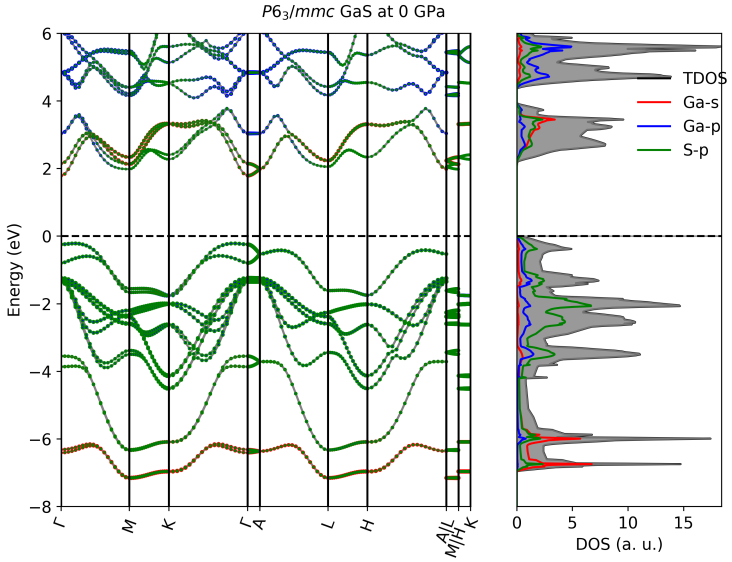
$P6_3/mmc$ GaS at 0 GPa
Energy (eV)
Γ
M
K
Γ
A
L
H
A|L
M|H
K
DOS (a. u.)
TDOS
Ga-s
Ga-p
S-p

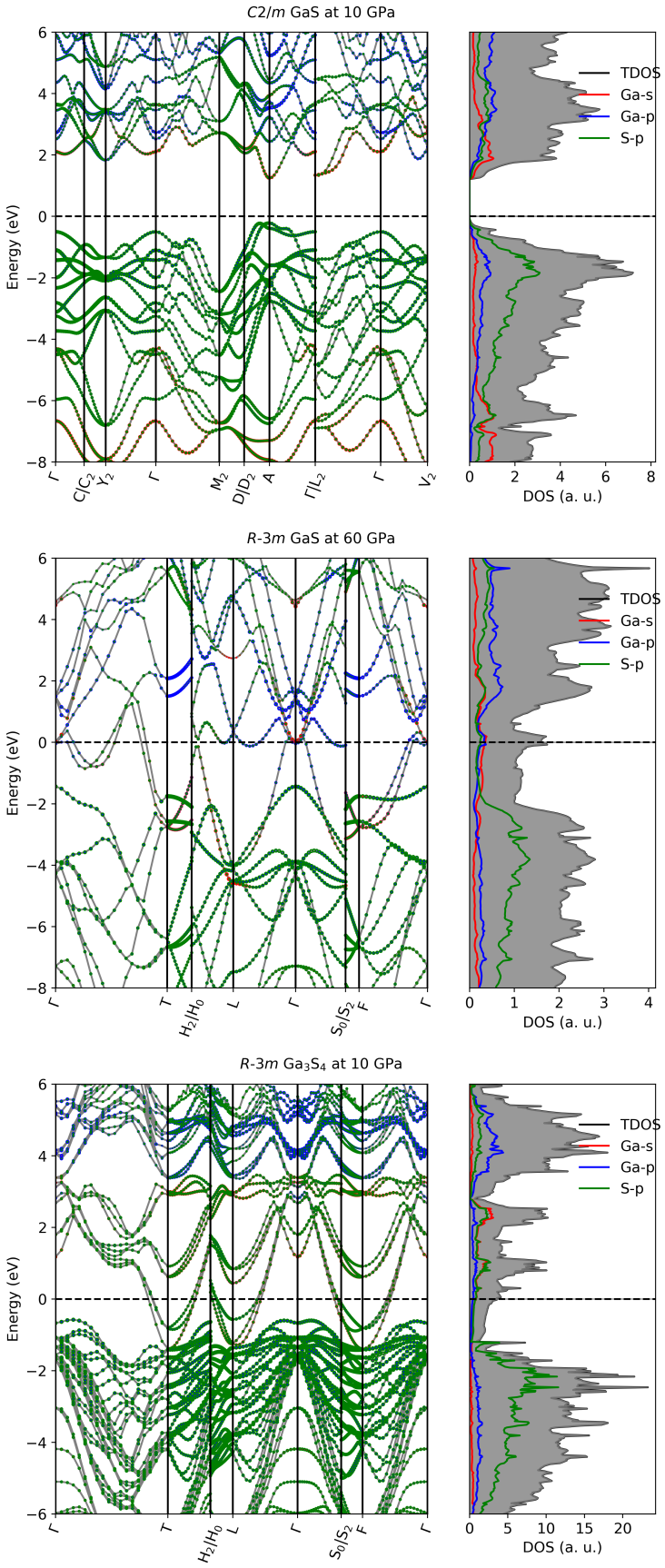
C2/m GaS at 10 GPa
Energy (eV)
Γ
C|C2
Y2
Γ
M2
D|D2
A
Γ|L2
Γ
V2
DOS (a. u.)
TDOS
Ga-s
Ga-p
S-p
R-3m GaS at 60 GPa
Energy (eV)
Γ
T
H2|H0
L
Γ
S0|S2
F
Γ
DOS (a. u.)
TDOS
Ga-s
Ga-p
S-p
R-3m Ga3S4 at 10 GPa
Energy (eV)
Γ
T
H2|H0
L
Γ
S0|S2
F
Γ
DOS (a. u.)
TDOS
Ga-s
Ga-p
S-p

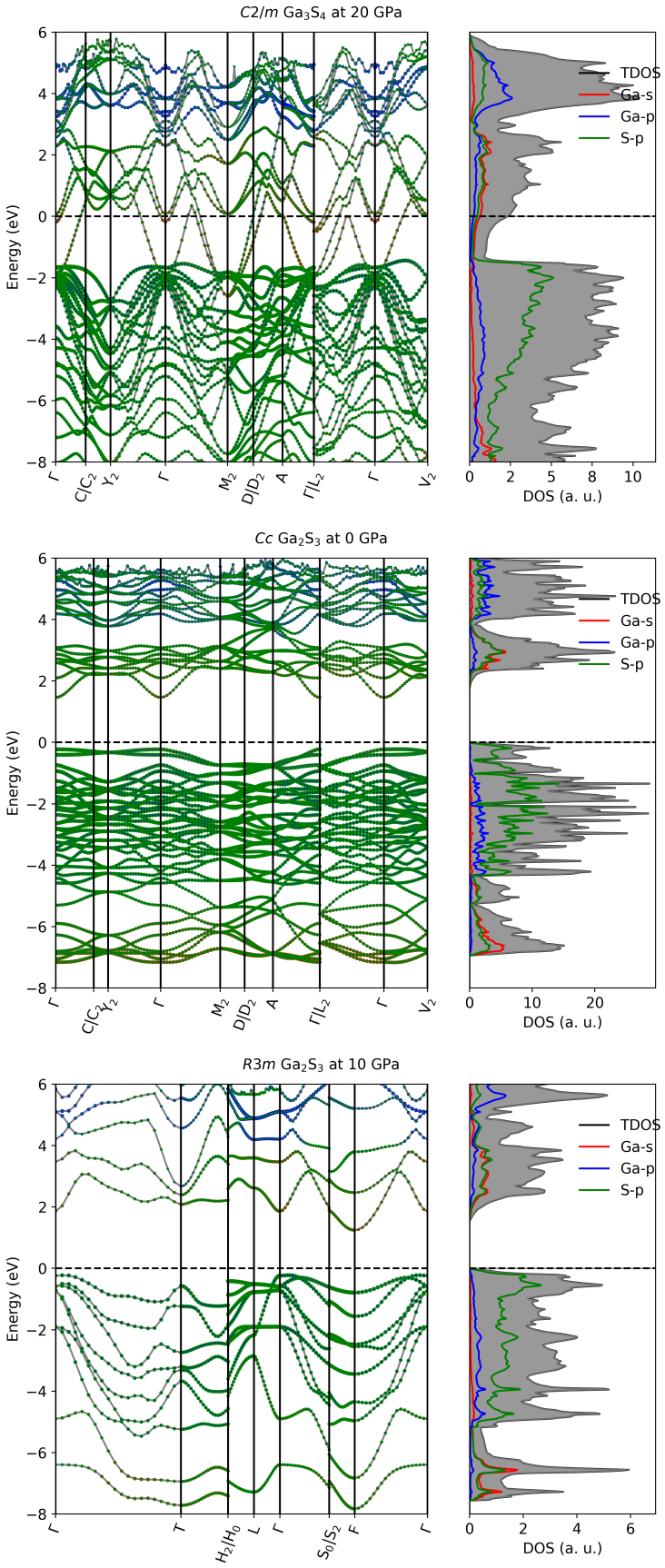
C2/m Ga3S4 at 20 GPa
Energy (eV)
Γ
C|C2
Y2
Γ
M2
D|D2
A
Γ|L2
Γ
V2
DOS (a. u.)
TDOS
Ga-s
Ga-p
S-p
Cc Ga2S3 at 0 GPa
Energy (eV)
Γ
C|C2
Y2
Γ
M2
D|D2
A
Γ|L2
Γ
V2
DOS (a. u.)
TDOS
Ga-s
Ga-p
S-p
R3m Ga2S3 at 10 GPa
Energy (eV)
Γ
T
H2|H0
L
Γ
S0|S2
F
Γ
DOS (a. u.)
TDOS
Ga-s
Ga-p
S-p

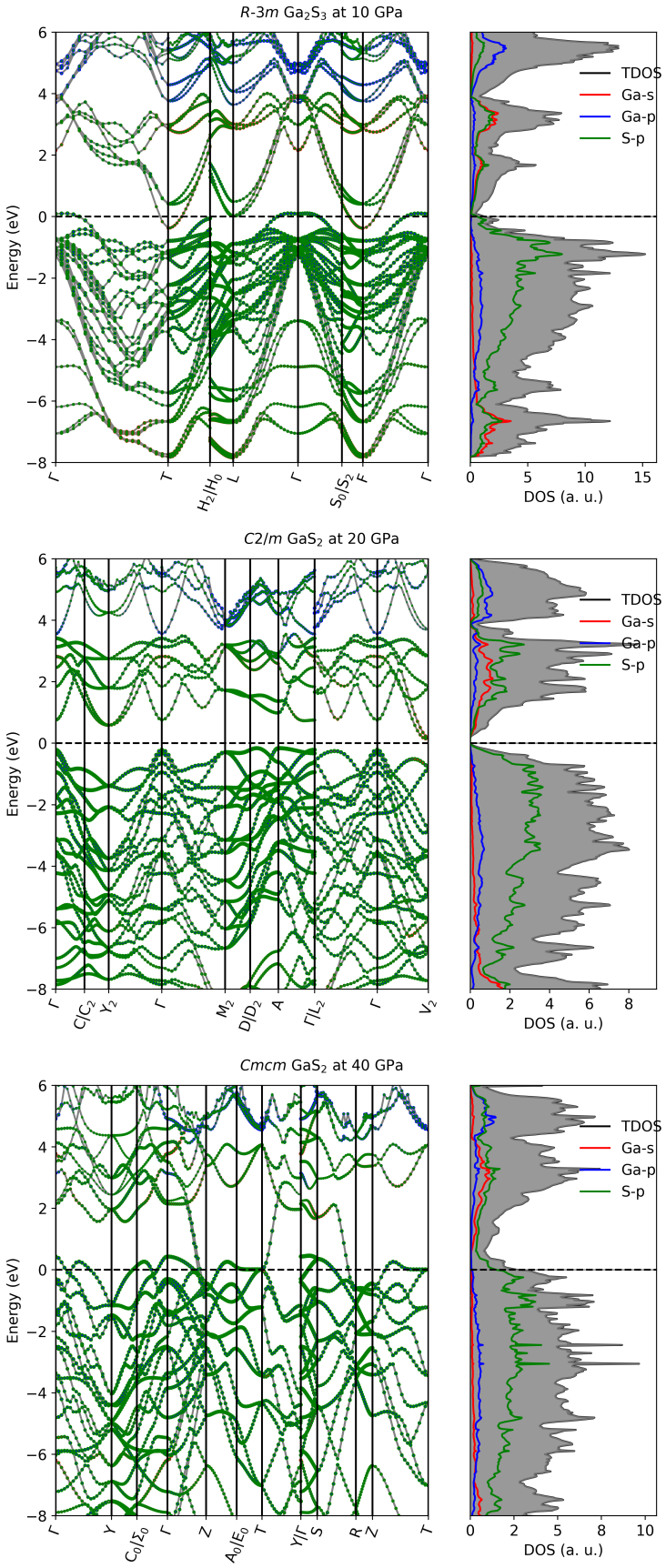
R-3m Ga2S3 at 10 GPa
Energy (eV)
Γ
T
H2|H0
L
Γ
S0|S2
F
Γ
DOS (a. u.)
TDOS
Ga-s
Ga-p
S-p
C2/m GaS2 at 20 GPa
Energy (eV)
Γ
C|C2
Y2
Γ
M2
D|D2
A
Γ|L2
Γ
V2
DOS (a. u.)
TDOS
Ga-s
Ga-p
S-p
Cmcm GaS2 at 40 GPa
Energy (eV)
Γ
Y
C0|Σ0
Γ
Z
A0|E0
T
Y|Γ
S
R
Z
T
DOS (a. u.)
TDOS
Ga-s
Ga-p
S-p

Quenchable phases

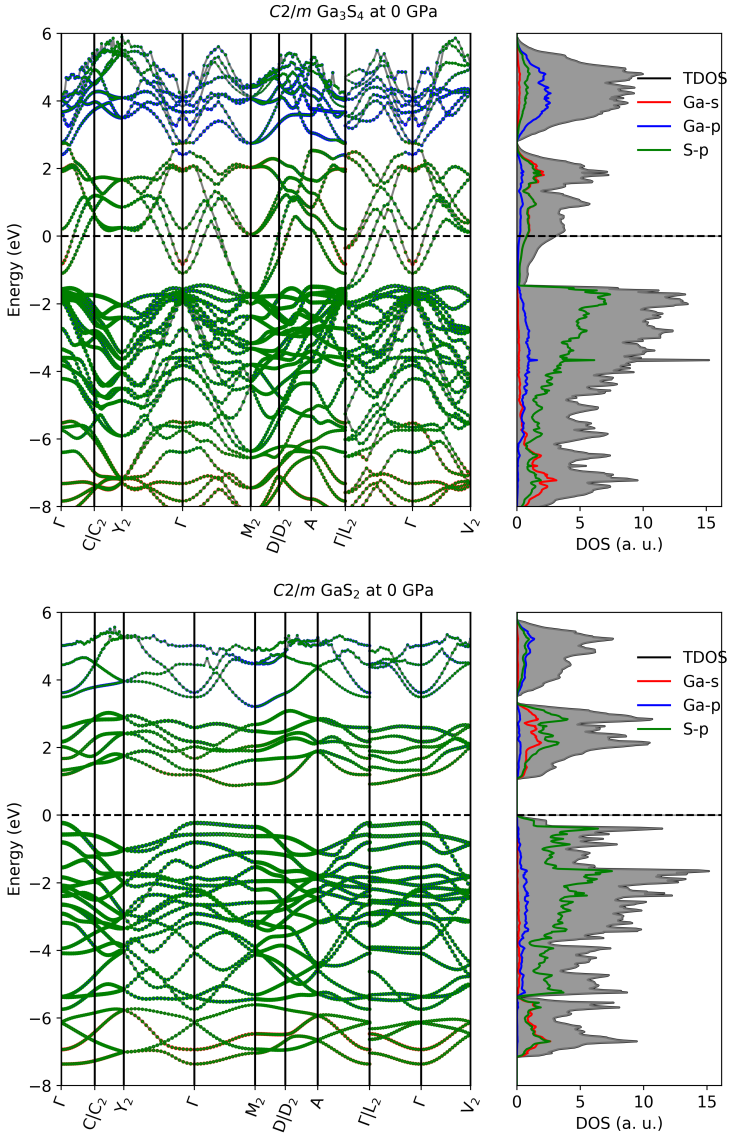

Figure S15: Band structures and DOS of Ga_xS_y at a given pressure (PBE level of theory).

S9 Bonding Analysis

In order to measure this electronic perturbation, we compute the COBIs of Ga-Ga, and Ga-S at the GGA-PBE level of theory. The COBI plot is presented in the figure S16 and the associated ICOBIs are given in the table S11.

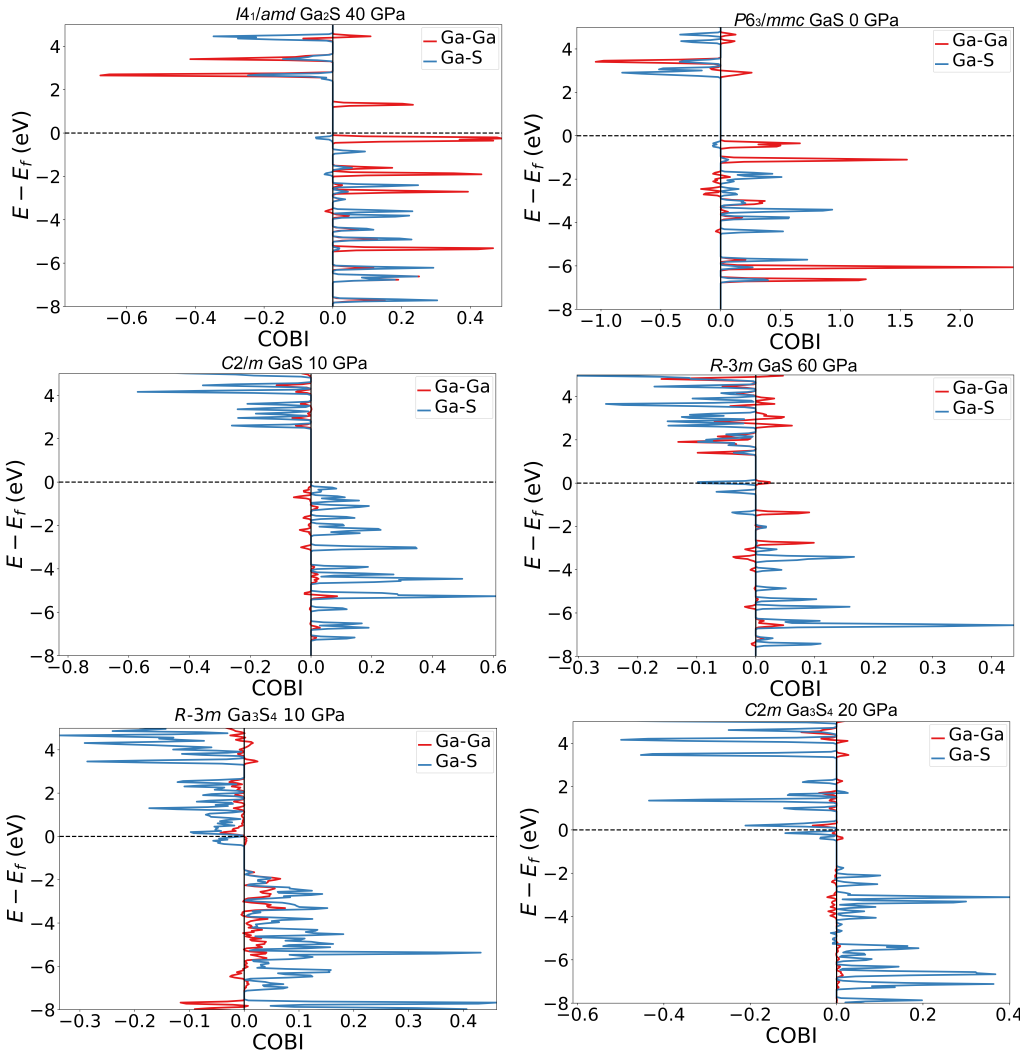

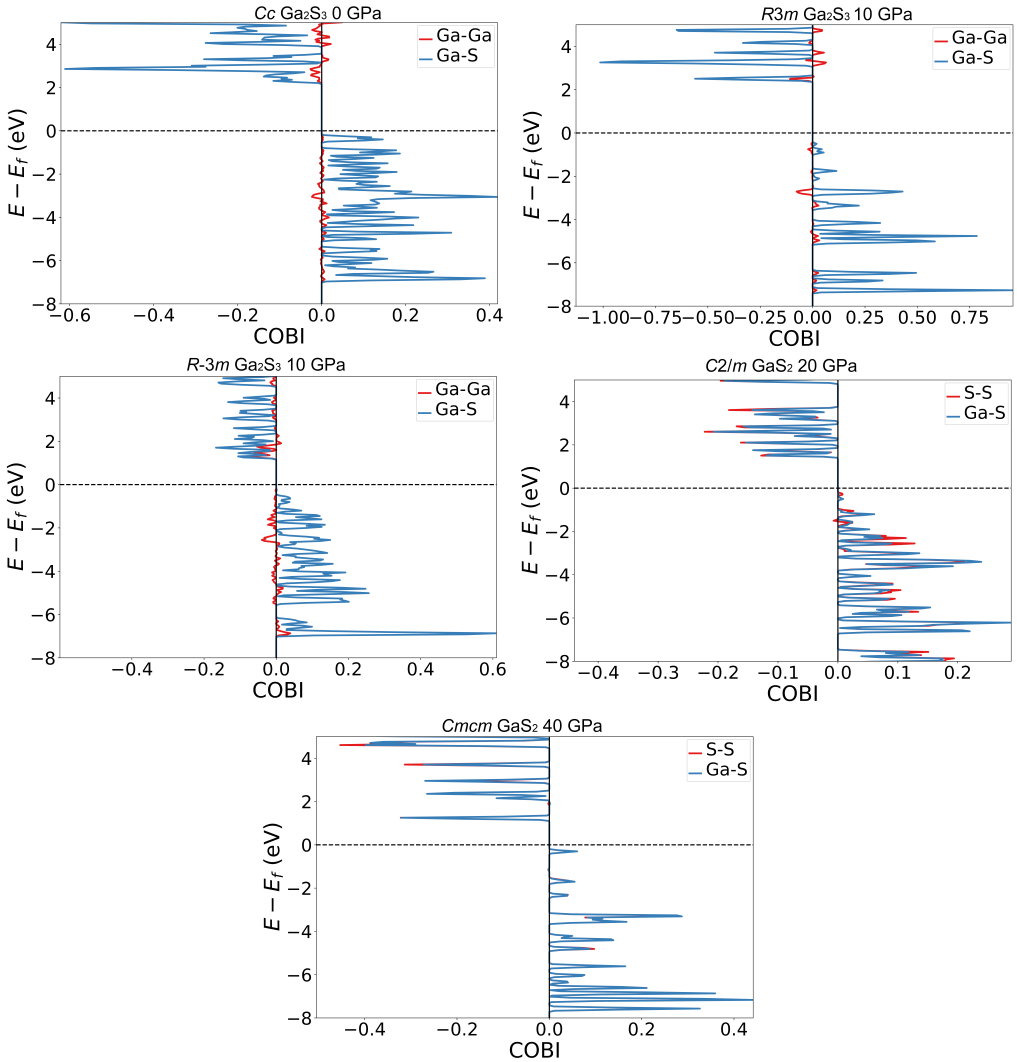

Quenchable phases

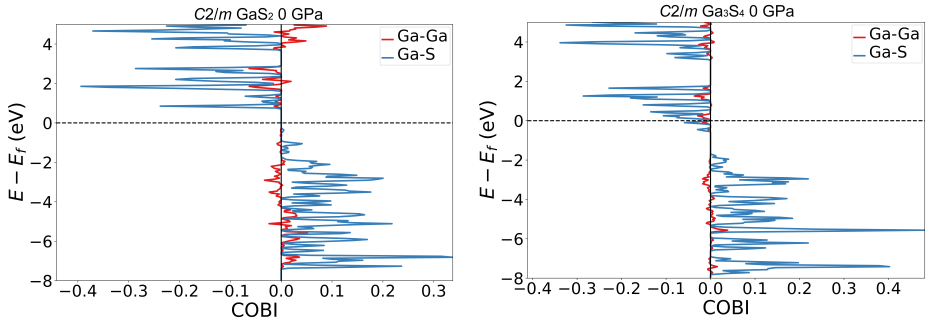

Figure S16: COBI plot of Ga_xS_y at a given pressure (PBE level of theory).

Table S11: ICOBIs for Predicted Ga-S Structures at PBE Level of Theory

Structure	**Pressure (GPa)**	**Space group**	**Bond**	**ICOBI**
Ga_2S	40	$I4_1/amd$ SG 141	Ga - Ga Ga - S	0.55 0.39
GaS	0	$P6_3/mmc$ SG 194	Ga - Ga Ga - S	0.81 0.80
GaS	10	C_2/m SG 12	Ga - Ga Ga - S	0.04 0.69
GaS	60	R-3m SG 166	Ga - Ga Ga - S	0.07 0.39
Ga_3S_4	10	R-3m SG 166	Ga - Ga Ga - S	0.06 0.73
Ga_3S_4	20	$C2/m$ SG 12	Ga - Ga Ga - S	0.04 0.52
Ga_2S_3	0	Cc SG 9	Ga - Ga Ga - S	0.03 0.99
Ga_2S_3	10	$R3m$ SG 160	Ga - Ga Ga - S	0.05 0.82
Ga_2S_3	10	R-3m SG 166	Ga - Ga Ga - S	0.05 0.73
GaS_2	20	$C2/m$ SG 12	S - S Ga - S	0.56 0.55
GaS_2	40	$Cmcm$ SG 63	S - S Ga - S	0.55 0.55
Quenchable				
Ga_3S_4	0	$C2/m$ SG 12	Ga - Ga Ga - S	0.03 0.59
GaS_2	0	$C2/m$ SG 12	S - S Ga - S	0.07 0.63

Table S12: Bader Charge and Formal Charge Values of Predicted Ga-S Structures at GGA-PBE Level of Theory

Structure	**Pressure (GPa)**	**Space group**	**Atom**	**Bader Charge (|e|)**	**Formal Charge (|e|)**
Ga_2S	40	$I4_1/amd$ SG 141	Ga S	+ 0.49 - 0.98	+ 1.2 - 2.4
GaS	0	$P6_3/mmc$ SG 194	Ga S	+ 0.81 - 0.81	+ 2.0 - 2.0
GaS	10	C_2/m SG 12	Ga S	+ 0.86 - 0.86	+ 2.1 - 2.1
GaS	60	R-3m SG 166	Ga S	+ 1.00 - 1.00	+ 2.4 - 2.4
Ga_3S_4	10	R-3m SG 166	Ga S	+ 1.14 - 0.85	+ 2.8 - 2.0
Ga_3S_4	20	$C2/m$ SG 12	Ga S	+ 1.15 - 0.86	+ 2.8 - 2.1
Ga_2S_3	0	Cc SG 9	Ga S	+ 1.20 - 0.80	+ 3.0 - 2.0
Ga_2S_3	10	$R3m$ SG 160	Ga S	+ 1.23 - 0.81	+ 3.0 - 2.0
Ga_2S_3	10	R-3m SG 166	Ga S	+ 1.22 - 0.85	+ 3.0 - 2.0
GaS_2	20	$C2/m$ SG 12	Ga_2S_2 S_2	+ 0.78 - 0.78	+ 1.9 - 1.9
GaS_2	40	$Cmcm$ SG 63	Ga_2S_2 S_∞	+ 0.82 - 0.82	+ 2.0 - 2.0

S10 Thermal Stabilities of Quenchable Ga_xS_y

S10.1 Thermal Stability of $C2/m$ Ga_3S_4.

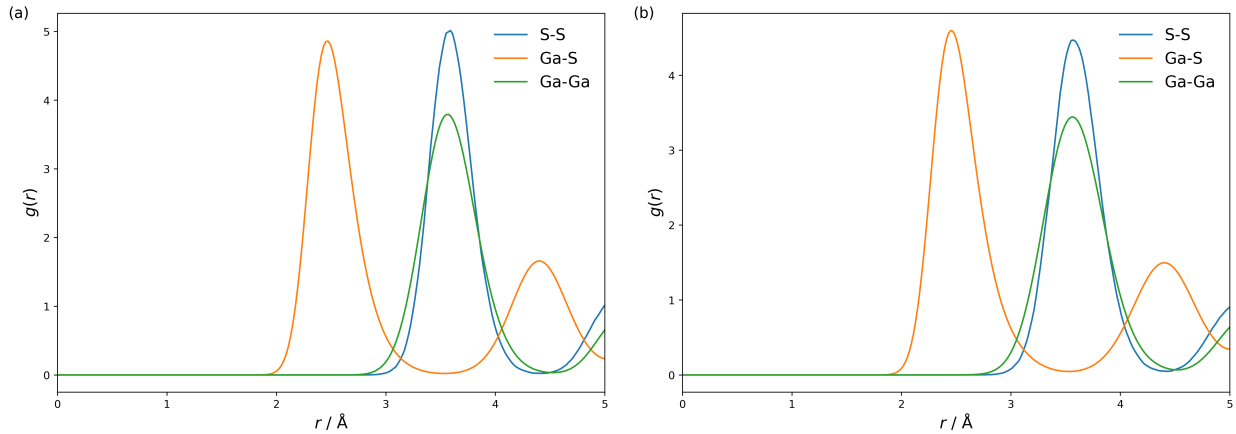

Figure S17: Radial distribution functions (RDF) of $C2/m$ Ga_3S_4 with 2x3x2 supercell (10 ps AIMD simulations) at (a) 800 K, and (b) 1000 K (PBE level of theory).

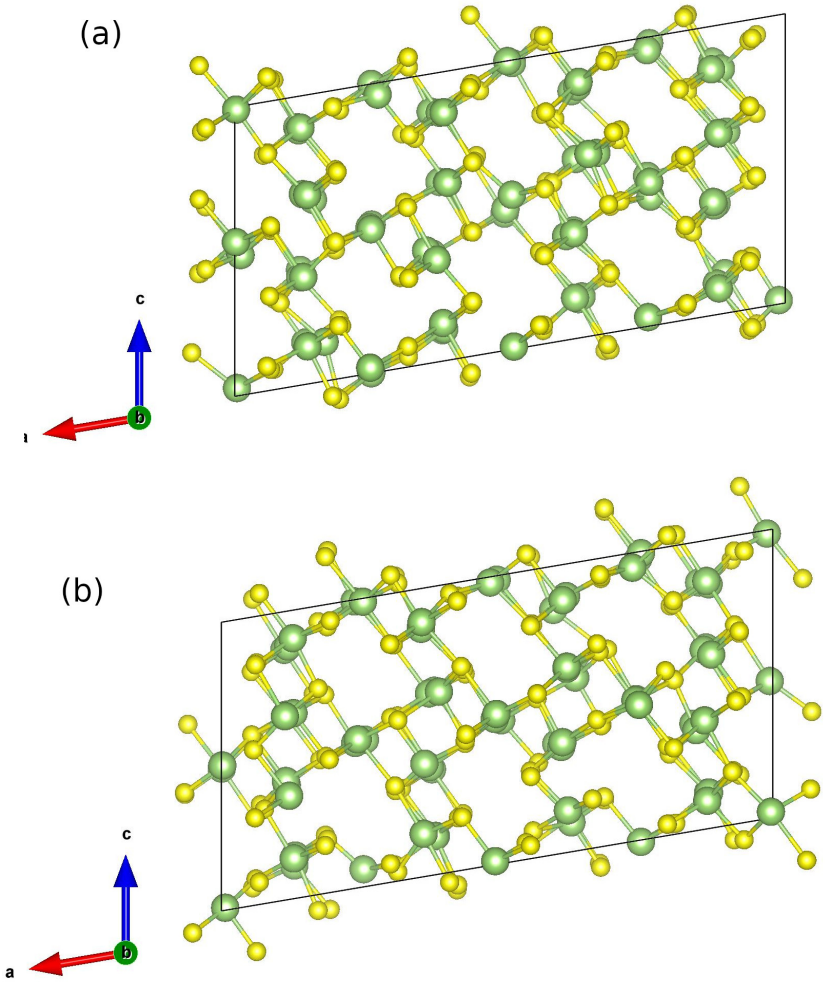

Figure S18: Snapshots of the $C2/m$ Ga_3S_4 with 2x3x2 supercell (10 ps AIMD simulations) at (a) 800 K and (b) 1000 K (PBE level of theory).

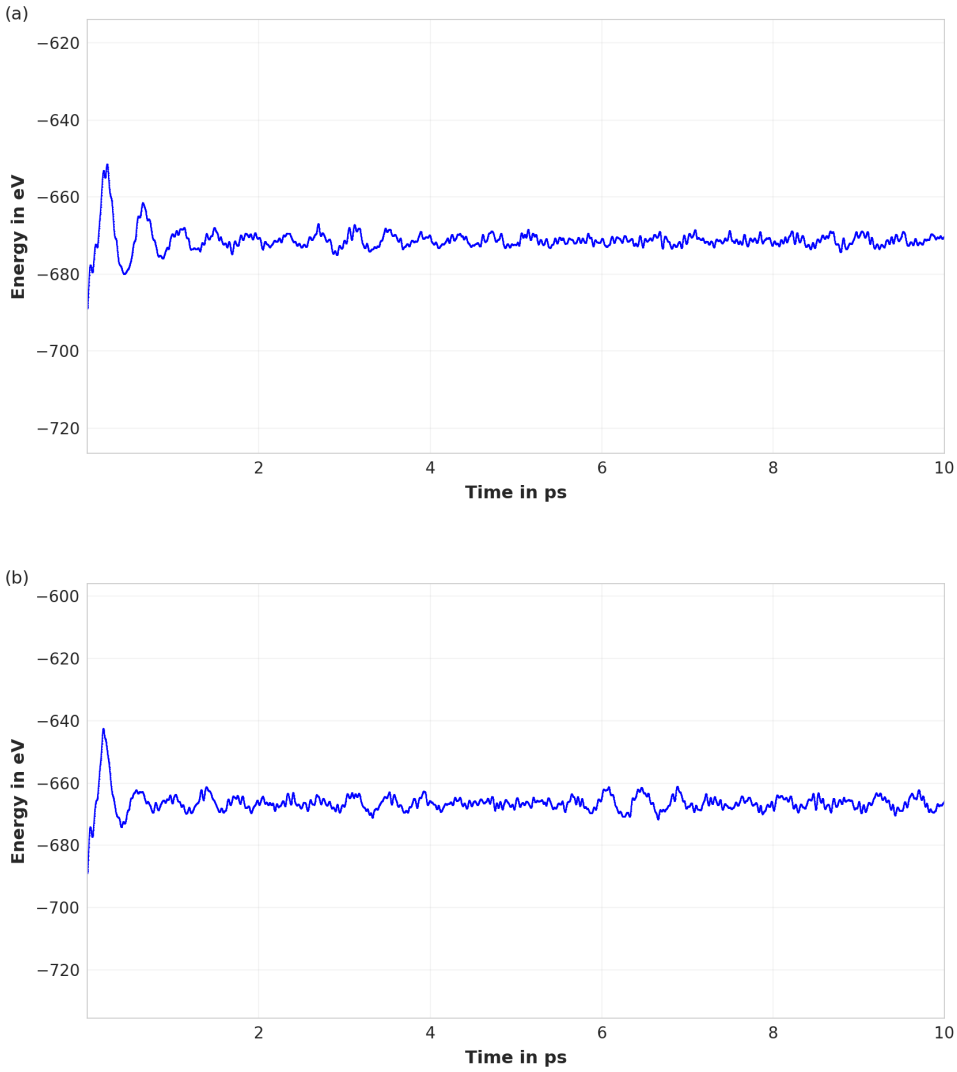

Figure S19: Energy in function of the time of $C2/m$ Ga_3S_4 with 2x3x2 supercell (10 ps AIMD simulations) at (a) 800 K and (b) 1000 K (PBE level of theory).

S10.2 Thermal Stability of $C2/m$ GaS_2.

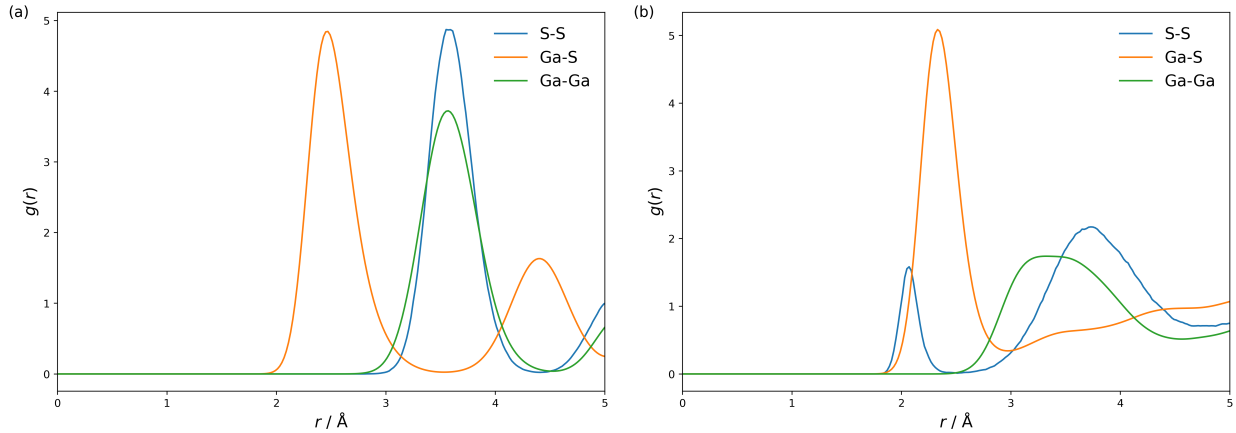

Figure S20: Radial distribution functions (RDF) of $C2/m$ GaS_2 with 2x3x2 supercell (10 ps AIMD simulations) at (a) 800 K, and (b) 1000 K (PBE level of theory).

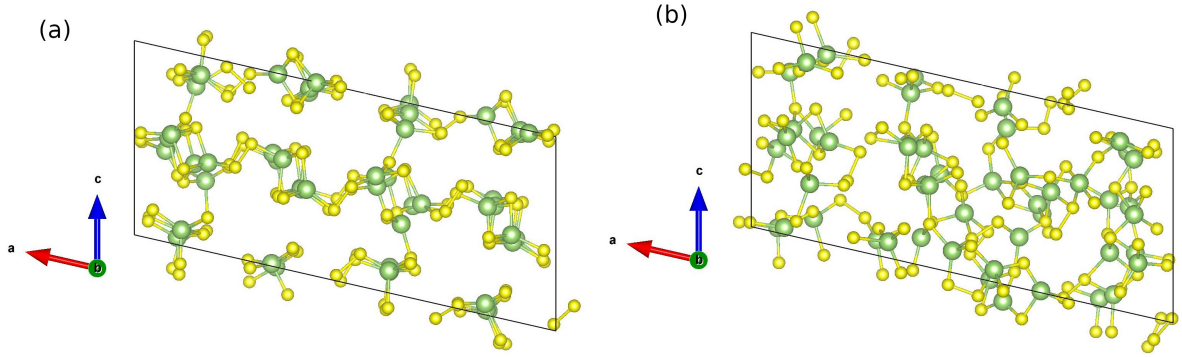

Figure S21: Snapshots of the $C2/m$ GaS_2 with 2x3x2 supercell (10 ps AIMD simulations) at (a) 800 K and (b) 1000 K (PBE level of theory).

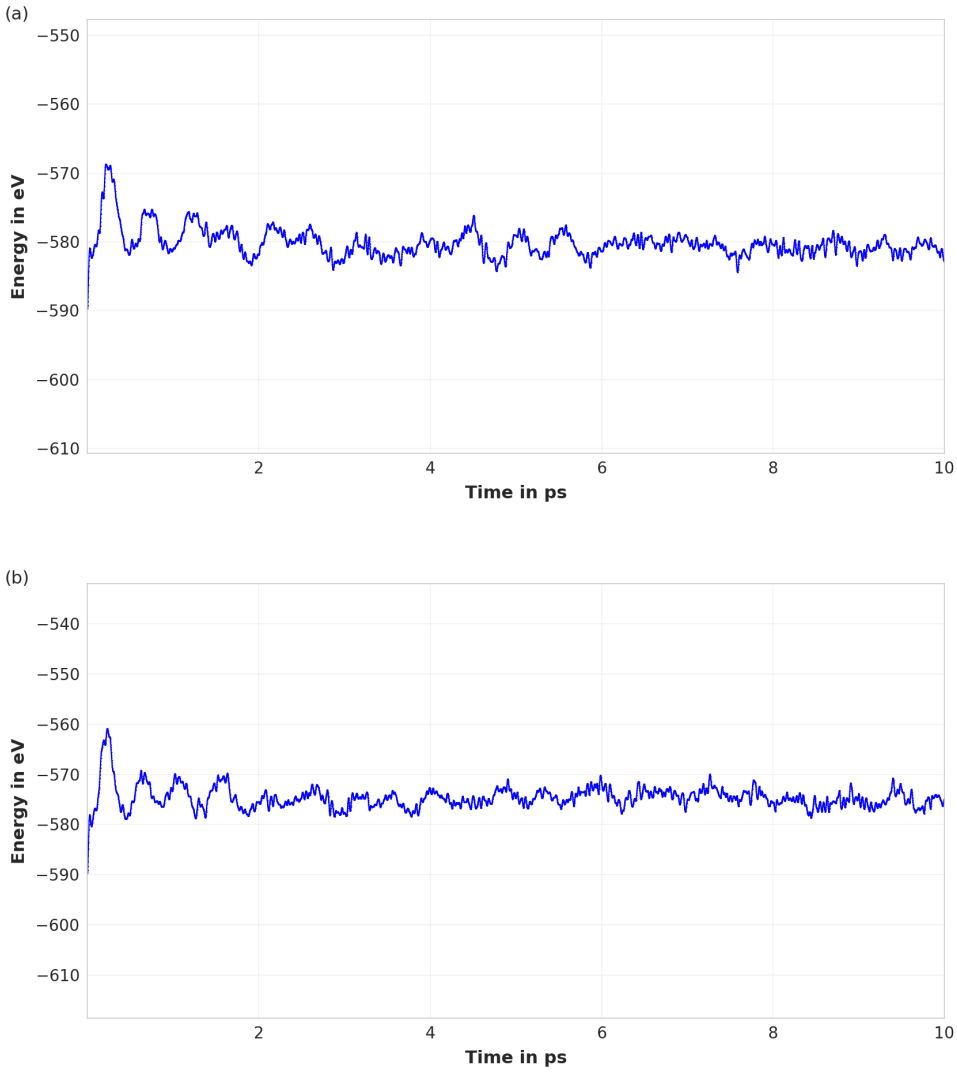

Figure S22: Energy in function of the time of $C2/m$ GaS_2 with 2x3x2 supercell (10 ps AIMD simulations) at (a) 800 K and (b) 1000 K (PBE level of theory).

S11 The Effect of Zero-Point Energy

The effect of zero-point energy (ZPE) on the stability of Ga-S compounds is studied. We find that the inclusion of ZPE only moderately shifts the stability figures but doesn't change the phase stability order.

Table S13: Formation Enthalpies Calculated for the Structures With and Without the Influence of Zero-Point Energy.

Phase	**Space group**	**Z**	**Formation enthalpies (without ZPE)**	**Formation enthalpies (with ZPE)**
Ga_2S	$I4_1/amd$ SG 141	4	-0.214	-0.208
GaS	$P6_3/mmc$ SG 194	4	-0.651	-0.644
Ga_3S_4	$C2/m$ SG 12	2	-0.492	-0.485
Ga_2S_3	Cc SG 9	4	-0.661	-0.650
GaS_2	$C2/m$ SG 12	4	-0.407	-0.397

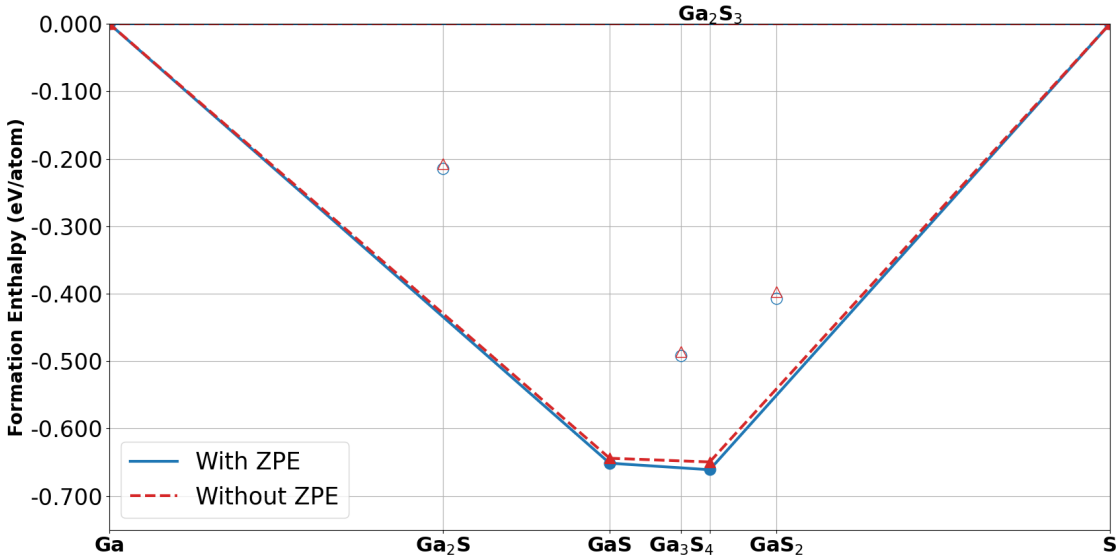

Figure S23: Convex-hull diagrams with and without ZPE correction (PBE level of theory) for the Ga-S system at 0 GPa.

S12 Energy Barrier and Transition Pathway in GaS_2

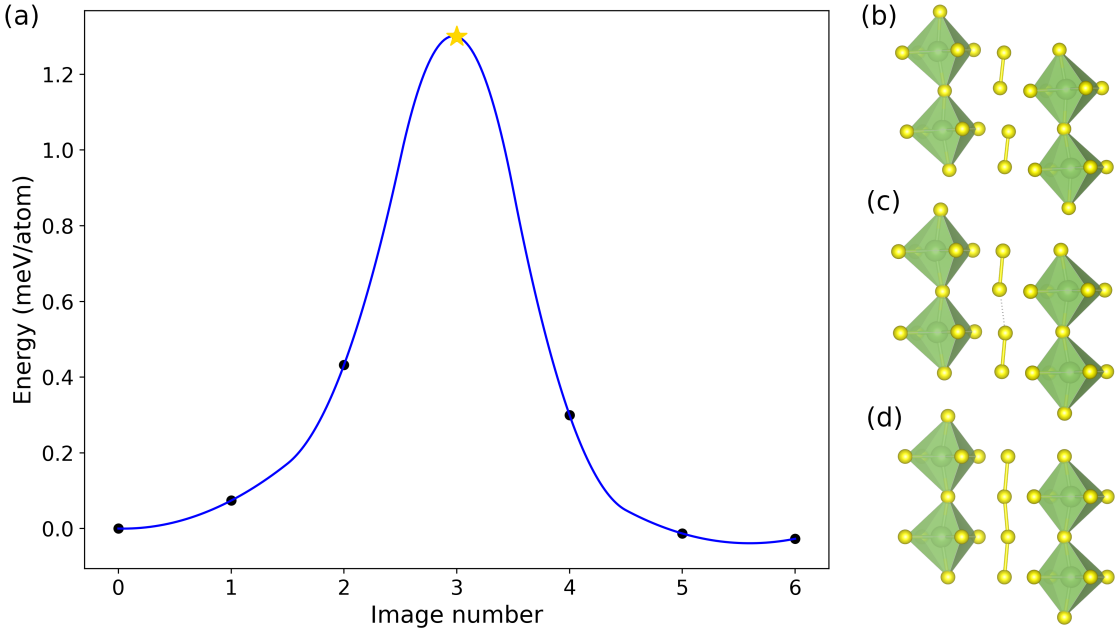

Figure S24: (a) Energy barrier calculated with the NEB method, the energy is relative to the initial state as a function of the image number between the initial and final state, (b) initial state structure $C2/m$ GaS_2 at 40 GPa, (c) Transition state GaS_2 at 40 GPa and (d) $Cmcm$ GaS_2 at 35 GPa.

S13 Stiffness Tensor

Table S14: Elastic Constants C_{ij} (GPa) in Bulk $P6_3/mmc$ GaS, $C2/m$ Ga_3S_4, Cc Ga_2S_3, $C2/m$ GaS_2 at PBE Level of Theory.

Structure	GaS	Ga_3S_4	Ga_2S_3	GaS_2
Space group	$P6_3/mmc$ SG 194	$C2/m$ SG 12	Cc SG 9	$C2/m$ SG 12
C_{11}	94	98	53	19
C_{12}	22	20	14	-7
C_{13}	1	24	19	-4
C_{14}	0	0	0	0
C_{15}	0	2	0	-3
C_{16}	0	0	0	0
C_{22}	94	140	49	125
C_{23}	1	36	14	-1
C_{24}	0	0	0	0
C_{25}	0	5	0	1
C_{26}	0	0	0	0
C_{33}	3	98	94	5
C_{34}	0	0	0	0
C_{35}	0	3	0	1
C_{36}	0	0	0	0
C_{44}	1	38	23	2
C_{45}	0	0	0	0
C_{46}	0	10	0	0
C_{55}	1	31	24	3
C_{56}	0	0	0	0
C_{66}	36	28	21	-2

Table S15: Born Stability Criteria for Selected Ga_xS_y Phases at 0 GPa. (Where g = $C_{11}C_{22}C_{33}$ + $2C_{12}C_{13}C_{23}$ - $C_{11}C_{23}^2$ - $C_{22}C_{13}^2$ - $C_{33}C_{12}^2$)

Structure	**Space group**	**Born Stability Criteria**	**Satisfied Born Criteria**
GaS	$P6_3/mmc$ SG 194	$C_{11} = 94 > \|C_{12}\| = 22$ $2C_{13}^2 = 2 < C_{33}(C_{11} + C_{12}) = 348$ $C_{44} = 1 > 0$	yes
Ga_3S_4	$C2/m$ SG 12	$C_{11} = 98 > 0$, $C_{22} = 140 > 0$, $C_{33} = 98 > 0$, $C_{44} = 38 > 0$, $C_{55} = 31 > 0$, $C_{66} = 28 > 0$ $C_{11} + C_{22} + C_{33} + 2(C_{12} + C_{13} + C_{23}) = 497 > 0$ $C_{33}\ C_{55} - C_{35}^2 = 3067 > 0$ $C_{44}\ C_{66} - C_{46}^2 = 977 > 0$ $C_{22} + C_{33} - 2C_{23} = 166 > 0$ $C_{22}(C_{33}C_{55} - C_{35}^2) + 2C_{23}C_{25}C_{35} - C_{23}^2C_{55} - C_{25}^2C_{33} = 386707 > 0$ $2[C_{15}C_{25}(C_{33}C_{12} - C_{13}C_{23}) + C_{15}C_{35}(C_{22}C_{13} - C_{12}C_{23}) +$ $C_{25}C_{35}(C_{11}C_{23} - C_{12}C_{13})] - [C_{15}^2(C_{22}C_{33} - C_{23}^2) +$ $C_{25}^2(C_{11}C_{33} - C_{13}^2) + C_{35}^2(C_{11}C_{22} - C_{12}^2)] + C_{55}*g = 35083309 > 0$	yes
Ga_2S_3	Cc SG 9	$C_{11} = 53 > 0$, $C_{22} = 49 > 0$, $C_{33} = 94 > 0$, $C_{44} = 23 > 0$, $C_{55} = 24 > 0$, $C_{66} = 21 > 0$ $C_{11} + C_{22} + C_{33} + 2(C_{12} + C_{13} + C_{23}) = 290 > 0$ $C_{33}\ C_{55} - C_{35}^2 = 2266 > 0$ $C_{44}\ C_{66} - C_{46}^2 = 482 > 0$ $C_{22} + C_{33} - 2C_{23} = 115 > 0$ $C_{22}(C_{33}C_{55} - C_{35}^2) + 2C_{23}C_{25}C_{35} - C_{23}^2C_{55} - C_{25}^2C_{33} = 106262 > 0$ $2[C_{15}C_{25}(C_{33}C_{12} - C_{13}C_{23}) + C_{15}C_{35}(C_{22}C_{13} - C_{12}C_{23}) +$ $C_{25}C_{35}(C_{11}C_{23} - C_{12}C_{13})] - [C_{15}^2(C_{22}C_{33} - C_{23}^2) +$ $C_{25}^2(C_{11}C_{33} - C_{13}^2) + C_{35}^2(C_{11}C_{22} - C_{12}^2)] + C_{55}*g = 4942365 > 0$	yes
GaS_2	$C2/m$ SG 12	$C_{11} = 19 > 0$, $C_{22} = 125 > 0$, $C_{33} = 5 > 0$, $C_{44} = 2 > 0$, $C_{55} = 3 > 0$, $C_{66} = -2 > 0$ $C_{11} + C_{22} + C_{33} + 2(C_{12} + C_{13} + C_{23}) = 125 > 0$ $C_{33}\ C_{55} - C_{35}^2 = 12 > 0$ $C_{44}\ C_{66} - C_{46}^2 = -5 > 0$ $C_{22} + C_{33} - 2C_{23} = 131 > 0$ $C_{22}(C_{33}C_{55} - C_{35}^2) + 2C_{23}C_{25}C_{35} - C_{23}^2C_{55} - C_{25}^2C_{33} = 1564 > 0$ $2[C_{15}C_{25}(C_{33}C_{12} - C_{13}C_{23}) + C_{15}C_{35}(C_{22}C_{13} - C_{12}C_{23}) +$ $C_{25}C_{35}(C_{11}C_{23} - C_{12}C_{13})] - [C_{15}^2(C_{22}C_{33} - C_{23}^2) +$ $C_{25}^2(C_{11}C_{33} - C_{13}^2) + C_{35}^2(C_{11}C_{22} - C_{12}^2)] + C_{55}*g = 20632 > 0$	no

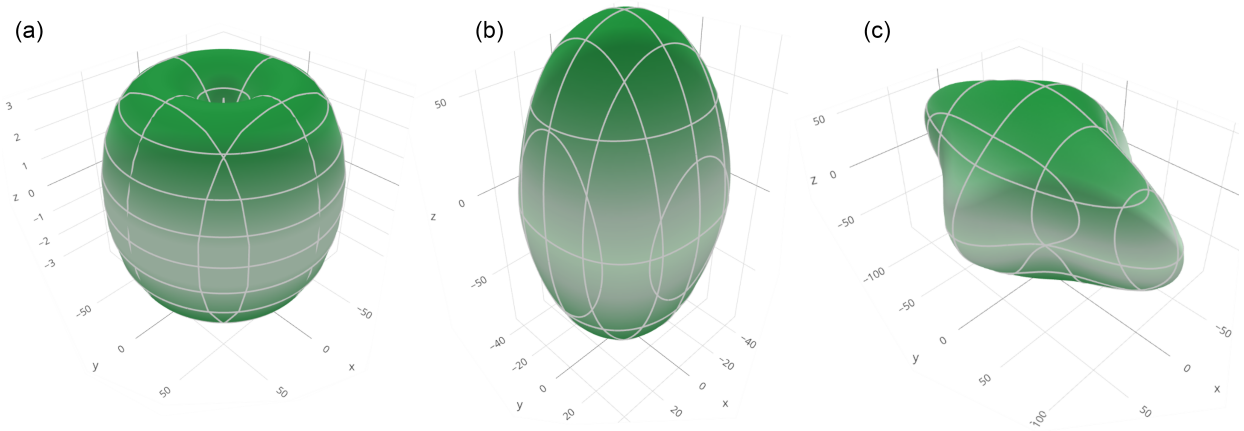

Figure S25: Directional dependence of Young's moduli (x, y, and z in GPa) for (a) $P6_3/mmc$ GaS, (b) Cc Ga_2S_3, (c) $C2/m$ Ga_3S_4

S14 Cleavage Energy

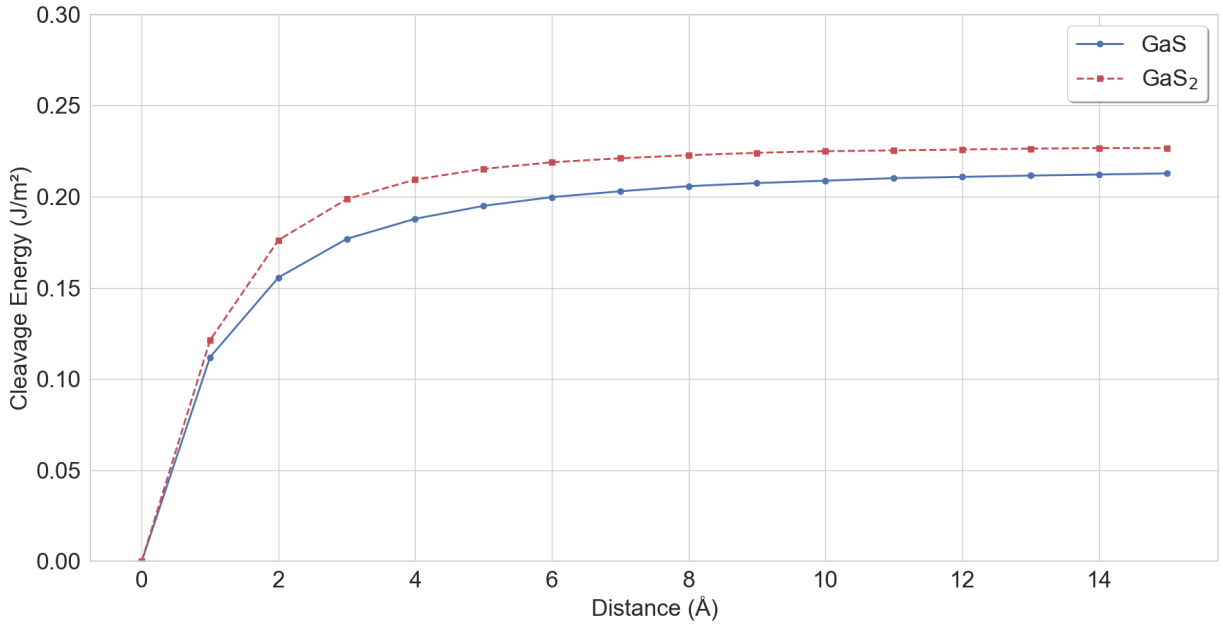

Figure S26: The cleavage energy calculated using the r^{2}SCAN+rVV10 functional as a function of the separation d between between two slabs.

To assess the feasibility of obtaining 2D GaS and GaS_2 slabs from their ground state bulk phases ($P6_3/mmc$ and $C2/m$, respectively), the cleavage energy (E_{cl}) was calculated as a function of the separation between two slabs:

$$E_{cl} = \frac{E - E_0}{S}$$

where E and E_0 are the energies of the separated state and the equilibrium state of the unit cell, respectively, and S is the surface area of the unit cell. A large interlayer separation was introduced to simulate fracture within the bulk (see inset of S26).

As shown in Figure S26, the calculated cleavage energies are 0.21 J m^{-2} for $P6_3/mmc$ GaS and 0.23 J m^{-2} for $C2/m$ GaS_2. These values are lower than that of graphene (0.37 J m^{-2})[34] and comparable to or lower than those of several other 2D materials-e.g., GeS (0.37 J m^{-2}),[35] FeS (0.26 J m^{-2}),[35] and MoS_2 (0.23 J m^{-2})[36])—suggesting that 2D GaS and GaS_2 slabs can be readily obtained via mechanical or liquid-phase exfoliation techniques.

S15 $C2/m$ Ga_3S_4 Phase, a Cation Vacancy Rock Salt-Type Structure.

From 15 to 55 GPa, Ga_3S_4 is thermodynamically stable and crystallizes in the monoclinic $C2/m$ space group (SG 12, Z = 2). The Ga atom is octahedrally coordinated to six sulfur atoms with Ga-S interatomic separations of 2.33 - 2.49 Å ($\sim$ 2.41 Å) at 20 GPa. The computed ICOBI value is 0.52, which highlights the delocalized character of the Ga-S bonding (see Table S11). The ELF plot serves to confirm this feature (See Figure S27). The sulfur atoms have two coordination modes: a 4 coordinated seahorse local environment and a 5-coordinated square-pyramidal configuration. From an ionic perspective, it is anticipated that each Ga atom will exhibit a charge of +2.7 when the sulfide S^{2-} is taken into account in Ga_3S_4. This is consistent with the mean formal charge of +2.8 derived from our Bader charge analysis (see Table S12). The structure of Ga_3S_4 can be viewed as a cation vacancy NaCl-type structure, namely $Ga_{(4\text{-}1)}S_4$. While ionic NaCl compound has a 4 valence electron count per atom, following the octet rule for AB binary system, the cation deficient $Ga_{(4\text{-}1)}S_4$ compound possesses an excess of electrons, i.e. 4.125 electron count per atom. Therefore, this high-pressure Ga_3S_4 phase is expected to be an electrical material. This feature is seen from the computed DOS in Figure S14; $C2/m$ Ga_3S_4 presents at the PBE level a closed band gap, and the Fermi level crosses a low density of states under pressure (see the band structure and the DOS of Ga_3S_4 in Figure S14).

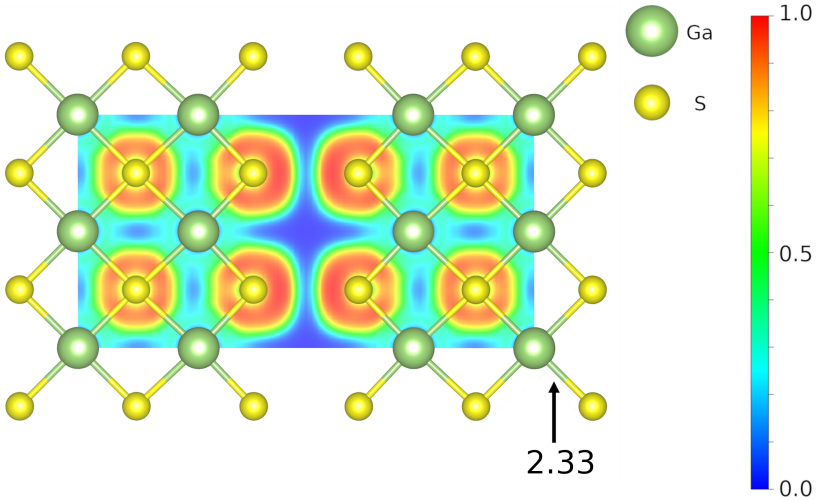

Figure S27: ELF plot of the plane 101 for $C2/m$ Ga_3S_4 at 20 GPa (PBE level of theory).

References

(1) Oganov, A. R.; Glass, C. W. Crystal Structure Prediction Using *Ab Initio* Evolutionary Techniques: Principles and Applications. *J. Chem. Phys.* **2006**, *124*, 244704.

(2) Oganov, A. R.; Lyakhov, A. O.; Valle, M. How Evolutionary Crystal Structure Prediction Works-and Why. *Acc. Chem. Res.* **2011**, *44*, 227–237.

(3) Lyakhov, A. O.; Oganov, A. R.; Stokes, H. T.; Zhu, Q. New Developments in Evolutionary Structure Prediction Algorithm USPEX. *Comput. Phys. Commun.* **2013**, *184*, 1172–1182.

(4) Zhou, X.-F.; Dong, X.; Oganov, A. R.; Zhu, Q.; Tian, Y.; Wang, H.-T. Semimetallic Two-Dimensional Boron Allotrope with Massless Dirac Fermions. *Phys. Rev. Lett.* **2014**, *112*, 085502.

(5) Kresse, G.; Furthmüller, J. Efficient Iterative Schemes for *Ab Initio* Total-Energy Calculations Using a Plane-Wave Basis Set. *Phys. Rev. B* **1996**, *54*, 11169.

(6) Kresse, G.; Furthmüller, J. Efficiency of *Ab-Initio* Total Energy Calculations for Metals and Semiconductors Using a Plane-Wave Basis Set. *Comput. Mater. Sci.* **1996**, *6*, 15–50.

(7) Blöchl, P. E. Projector Augmented-Wave Method. *Phys. Rev. B* **1994**, *50*, 17953.

(8) Kresse, G.; Joubert, D. From Ultrasoft Pseudopotentials to the Projector Augmented-wave Method. *Phys. Rev. B* **1999**, *59*, 1758–1775.

(9) Perdew, J. P.; Burke, K.; Ernzerhof, M. Generalized Gradient Approximation Made Simple. *Phys. Rev. Lett.* **1996**, *77*, 3865–3868.

(10) Pickard, C. J.; Needs, R. J. High-Pressure Phases of Silane. *Phys. Rev. Lett.* **2006**, *97*, 045504.

(11) Pickard, C. J.; Needs, R. J. *Ab initio* Random Structure Searching. *J. Phys.: Condens. Matter* **2011**, *23*, 053201.

(12) Pickard, C. J. Ephemeral Data Derived Potentials for Random Structure Search. *Phys. Rev. B* **2022**, *106*, 014102.

(13) Sabatini, R.; Gorni, T.; de Gironcoli, S. Nonlocal van der Waals Density Functional Made Simple and Efficient. *Phys. Rev. B* **2013**, *87*, 041108.

(14) Peng, H.; Yang, Z.-H.; Perdew, J. P.; Sun, J. Versatile van der Waals Density Functional Based on a Meta-Generalized Gradient Approximation. *Phys. Rev. X* **2016**, *6*, 041005.

(15) Sun, J.; Ruzsinszky, A.; Perdew, J. P. Strongly Constrained and Appropriately Normed Semilocal Density Functional. *Phys. Rev. Lett.* **2015**, *115*, 036402.

(16) Furness, J. W.; Kaplan, A. D.; Ning, J.; Perdew, J. P.; Sun, J. Accurate and Numerically Efficient r^{2}SCAN Meta-Generalized Gradient Approximation. *J. Phys. Chem. Lett.* **2020**, *11*, 8208–8215.

(17) Togo, A.; Chaput, L.; Tadano, T.; Tanaka, I. Implementation Strategies in Phonopy and Phono3py. *J. Phys. Condens. Matter* **2023**, *35*, 353001.

(18) Togo, A. First-principles Phonon Calculations with Phonopy and Phono3py. *J. Phys. Soc. Jpn.* **2023**, *92*, 012001.

(19) Born, M.; Huang, K.; Lax, M. Dynamical Theory of Crystal Lattices. *Am. J. Phys.* **1955**, *23*, 474–474.

(20) Mouhat, F.; Coudert, F.-X. Necessary and Sufficient Elastic Stability Conditions in Various Crystal Systems. *Phys. Rev. B* **2014**, *90*, 224104.

(21) Cowley, R. A. Acoustic Phonon Instabilities and Structural Phase Transitions. *Phys. Rev. B* **1976**, *13*, 4877–4885.

(22) Silvi, B.; Savin, A. Classification of Chemical Bonds Based on Topological Analysis of Electron Localization Functions. *Nature* **1994**, *371*, 683–686.

(23) Momma, K.; Izumi, F. VESTA 3 for Three-Dimensional Visualization of Crystal, Volumetric and Morphology Data. *J. Appl. Crystallogr.* **2011**, *44*, 1272–1276.

(24) Krukau, A. V.; Vydrov, O. A.; Izmaylov, A. F.; Scuseria, G. E. Influence of the Exchange Screening Parameter on the Performance of Screened Hybrid Functionals. *J. Chem. Phys.* **2006**, *125*, 224106.

(25) Müller, P. C.; Ertural, C.; Hempelmann, J.; Dronskowski, R. Crystal Orbital Bond Index: Covalent Bond Orders in Solids. *J. Phys. Chem. C* **2021**, *125*, 7959–7970.

(26) Maintz, S.; Deringer, V. L.; Tchougréeff, A. L.; Dronskowski, R. LOBSTER: A Tool to Extract Chemical Bonding from Plane-wave Based DFT. 2016.

(27) Nelson, R.; Ertural, C.; George, J.; Deringer, V. L.; Hautier, G.; Dronskowski, R. LOBSTER: Local Orbital Projections, Atomic Charges, and Chemical-Bonding Analysis from Projector-Augmented-Wave-Based Density-Functional Theory. *J. Comput. Chem.* **2020**, *41*, 1931–1940.

(28) Jain, A.; Ong, S. P.; Hautier, G.; Chen, W.; Richards, W. D.; Dacek, S.; Cholia, S.; Gunter, D.; Skinner, D.; Ceder, G.; Persson, K. A. Commentary: The Materials Project: A Materials Genome Approach to Accelerating Materials Innovation. *APL Mater.* **2013**, *1*, 011002.

(29) Degtyareva, O.; McMahon, M. I.; Allan, D. R.; Nelmes, R. J. Structural Complexity in Gallium under High Pressure: Relation to Alkali Elements. *Phys. Rev. Lett.* **2004**, *93*, 205502.

(30) Weir, C. E.; Piermarini, G. J.; Block, S. On the Crystal Structures of Cs II and Ga II. *The Journal of Chemical Physics* **1971**, *54*, 2768–2770.

(31) Rettig, S. J.; Trotter, J. Refinement of the Structure of Orthorhombic Sulfur, α-S_8. *Acta Crystallogr., Sect. C: Cryst. Struct. Commun.* **1987**, *43*, 2260–2262.

(32) Crapanzano, L.; Crichton, W. A.; Monaco, G.; Bellissent, R.; Mezouar, M. Alternating Sequence of Ring and Chain Structures in Sulphur at High Pressure and Temperature. *Nature Mater.* **2005**, *4*, 550–552.

(33) McMahon, M. I.; Nelmes, R. J. High-Pressure Structures and Phase Transformations in Elemental Metals. *Chem. Soc. Rev.* **2006**, *35*, 943.

(34) Wang, W.; Dai, S.; Li, X.; Yang, J.; Srolovitz, D. J.; Zheng, Q. Measurement of the Cleavage Energy of Graphite. *Nature Commun.* **2015**, *6*, 7853.

(35) Li, F.; Liu, X.; Wang, Y.; Li, Y. Germanium Monosulfide Monolayer: a Novel Two-Dimensional Semiconductor with a High Carrier Mobility. *J. Mater. Chem. C* **2016**, *4*, 2155–2159.

(36) Yang, L.; Wang, D.; Liu, M.; Liu, H.; Tan, J.; Wang, Z.; Zhou, H.; Yu, Q.; Wang, J.; Lin, J.; Zou, X.; Qiu, L.; Cheng, H.-M.; Liu, B. Glue-Assisted Grinding Exfoliation of Large-Size 2D Materials for Insulating Thermal Conduction and Large-Current-Density Hydrogen Evolution. *Mater. Today* **2021**, *51*, 145–154.